Eur. Phys. J. A (2025) 61:280
https://doi.org/10.1140/epja/s10050-025-01759-3

THE EUROPEAN PHYSICAL JOURNAL A

Review

The status of $^{12}C+^{12}C$ fusion process

Alessandro Chieffi[1,2,3], Sandrine Courtin[4], R. James deBoer[5,a], Rosanna Depalo[6,7], Alexis Diaz-Torres[8], A. Di Leva[9,10], Thibaut Dumont[4], Federico Ferraro[11], Riccardo Maria Gesuè[11,12], Marcel Heine[4], G. Imbriani[9,10], Marco La Cognata[13], Aliya Nurmukhanbetova[13,14], Alessandro Oliva[13], Lorenzo Roberti[15,16], Roberta Spartá[13,14], Alexandra Spiridon[17], Wanpeng Tan[5], Xiaodong Tang[18,19], Livius Trache[17], Aurora Tumino[13,14], Michael Wiescher[5,b]

[1] Istituto Nazionale di Astrofisica—Istituto di Astrofisica e Planetologia Spaziali, Via Fosso del Cavaliere 100, 00133 Rome, Italy
[2] INFN. Sezione di Perugia, Via A. Pascoli s/n, 06125 Perugia, Italy
[3] Monash Centre for Astrophysics (MoCA), School of Mathematical Sciences, Monash University, Victoria 3800, Australia
[4] Université de Strasbourg, CNRS, IPHC UMR 7178, 67000 Strasbourg, France
[5] Department of Physics and Astronomy, University of Notre Dame, Notre Dame, IA 46556, USA
[6] Universitá degli Studi di Milano, Via G. Celoria 16, 20133 Milan, Italy
[7] INFN, Sezione di Milano, Via G. Celoria 16, 20133 Milan, Italy
[8] Department of Physics, University of Surrey, Guildford GU2 7XH, England, UK
[9] Universita degli Studi di Napoli "Federico II", Dipartimento di Fisica "E. Pancini", Via Cintia, 80126 Naples, Italy
[10] INFN, Sezione di Napoli, Via Cintia, 80126 Naples, Italy
[11] INFN-Laboratori Nazionali del Gran Sasso, Via Giovanni Acitelli 22, 67100 L'Aquila, Italy
[12] Gran Sasso Science Institute, Viale Francesco Crispi 7, 67100 L'Aquila, Italy
[13] INFN-Laboratori Nazionali del Sud, Via S. Sofia 62, 95123 Catania, Italy
[14] Dipartimento di Ingegneria e Architettura, Università degli Studi di Enna "Kore", Cittadella Universitaria, Enna, Italy
[15] Konkoly Observatory, Research Centre for Astronomy and Earth Sciences, HUN-REN, Konkoly Thege Miklós út 15-17, Budapest 1121, Hungary
[16] CSFK HUN-REN, MTA Centre of Excellence, Konkoly Thege Miklós út 15-17, Budapest 1121, Hungary
[17] Horia Hulubei National Institute for R&D in Physics and Nuclear Engineering, Bucharest-Magurele, Romania
[18] Institute of Modern Physics, Chinese Academy of Sciences, 509 Nanchang Rd., Lanzhou 730000, China
[19] Joint department of nuclear physics, Lanzhou University and Institute of Modern Physics, Lanzhou 730000, China

Received: 14 January 2025 / Accepted: 23 November 2025

Communicated by David Blaschke

Abstract This review summarizes the state of knowledge of the $^{12}C+^{12}C$ fusion reaction and its impact on stellar carbon burning environments.

Contents

[a] e-mail: Richard.J.deBoer.12@nd.edu (corresponding author)
[b] e-mail: wiescher.1@nd.edu

1 Introduction

The $^{12}C+^{12}C$ reaction is one of the most intriguing reactions in the field of nuclear astrophysics. The presently existing predictions of the reaction rates at stellar temperatures carry enormous uncertainties, which include the possibility of hindrance effects in the fusion process [1,2] as well as the observation of pronounced resonances in the low-energy range near the fusion threshold [3]. The hindrance effect, suggested to cause an additional reduction in the probability of fusion towards lower energies due to the incompressibility of nuclear matter [4], is still a matter of debate. The available experimental data do not reach the energy range where

Published online: 11 December 2025

hindrance becomes uniquely observable, and the extrapolation depends on the model assumptions. Resonance features are observed directly in low-energy fusion studies [5–7] and emerge in a very pronounced manner in indirect fusion studies labeled as Trojan Horse Method (THM) [3]. The nature of these resonances remains an enigma: are they traditional compound resonance states linking the fusion channel to the various exit channels such as proton, alpha, and gamma emission of highly excited levels in the compound system ^{24}Mg, or are they reflections of complex dynamic quantum coupling mechanisms occurring during the fusion process [8]? It may also be possible that the transfer reactions associated with the indirect THM approach populate high-spin states. At lower energies, the high orbital momentum barrier prevents these states from influencing the ^{12}C+^{12}C fusion reaction, but errors in the spin parity assignment could lead to an over estimation of the reaction rate. Therefore, achieving a precise understanding of the spin and parity of the observed levels by using THM becomes essential to delineate their specific role in the fusion process. This approach will be discussed in more detail in Sect. 5.1.

In summary, the physics underlying the low-energy fusion process is still largely unknown, and despite several modeling and experimental attempts to push the direct reaction studies towards the unknown energy range of stellar environments, the full impact of the reaction remains unknown as well. The actual fusion mechanism is not only a problem for the reaction under consideration but may also impact the prediction of other light-ion fusion reactions such as ^{16}O+^{16}O during later burning stages and fusion reactions between neutron-rich isotopes as anticipated for the deeper crust of accreting neutron stars [9]. Despite numerous modeling efforts described in sect 6, the complete impact of these reactions on critical carbon-burning environments remains uncertain.

The ^{12}C+^{12}C fusion reaction is thought to play a key role in three stellar burning environments. It drives the carbon burning phase of massive stars during late stellar evolution, converting the ^{12}C abundances to ^{20}Ne and ^{23}Na, with the latter subsequently converted to ^{20}Ne as well via ^{23}Na$(p,\alpha)^{20}$Ne [10–13]. Subsequent proton and alpha capture reactions could feed the Mg Si mass range. The abundance of ^{16}O produced during the preceding helium-burning phase remains largely undisturbed [14], although, depending on the reaction rate and on the ^{16}O/^{12}C abundance ratio, the ^{16}O+^{12}C fusion may play a minor role toward the end of the carbon burning phase [15,16].

The ^{12}C+^{12}C fusion has always been considered as the most likely ignition process for type Ia thermonuclear supernovae in accreting or merging carbon-oxygen or hybrid carbon-oxygen-neon white dwarfs [17–20]. Fusion occurs gradually through deflagration of a carbon burning zone at high densities, which eventually triggers the ignition driven by the rapid conversion of the ^{12}C and ^{16}O fuel to ^{56}Ni in statistical equilibrium. For determining the ignition point, knowledge of the fusion rate is of particular importance, as is the density of the white dwarf environment, which sets the electron screening conditions and enhancement for the fusion environment [21].

Interest in the role of the ^{12}C+^{12}C fusion reaction was further amplified with the suggestion that the observation of superbursts, extended thermonuclear explosions in the crust of accreting neutron stars, are driven by a single resonance in the ^{12}C+^{12}C fusion process [22–26], predicted for the lower, barely explored energy range [19,27]. This would point to the importance of low-energy resonances in the fusion process, but again, high density conditions in the neutron star crust would determine the fusion enhancement through electron screening [21].

In the following, we will focus on the early ^{12}C+^{12}C fusion studies, which introduced the ideas of molecular resonances and fusion hindrance as summarized in Sect. 2. This will be followed by a summary of recent experiments, which tried to expand the method towards lower energies by using a number of complementary experimental techniques as described in 3. In the following Sect. 4 new experimental developments towards pushing the cross section measurements towards the Gamow range are being discussed and evaluated. The experimental effort needs to be complemented by theoretical modeling to understand and explain the mechanism of fusion processes at low energies near the ^{12}C+^{12}C threshold [28]. The more recent theoretical modeling attempts are summarized in Sect. 6. Finally, the last Sect. 7 concentrates on the impact of the ^{12}C+^{12}C fusion rate on the nuclosynthesis pattern during late stellar evolution. At these conditions the nuclear physics aspect in the fusion rate has its largest impact since it is not dominated by strong electron screening effects. Electron screening diminishes the effective Coulomb barrier and causes a dramatic enhancement in the fusion reaction in high-density white dwarf or neutron star environments. Electron screening is not the subject of this review and the authors refer to earlier summaries of electron screening in heavy ion fusion reactions [21,28,29]

2 Early reaction studies in ^{12}C+^{12}C

The study of light-ion fusion reactions emerged as an important research field in the 1950s as a side product of the nuclear test program associated with the development of the hydrogen bomb [30–33]. These early studies have triggered broader interest with the results of low-energy fusion reactions of carbon isotopes, which suggested a pronounced and rather unexpected resonance pattern. This had not been observed in previous light-ion fusion studies [33,34], but was confirmed by measurements of the elastic scattering channel [35]. Initially, the reaction cross sections were discussed in

the framework of statistical model calculations [36,37], but subsequent experiments [38–40] supported the existence of pronounced resonance structures. This kind of low-energy resonances may provide an explanation for the observed enhancement in the low-energy cross section, a phenomenon initially dubbed absorption below the barrier, which was predicted to cause a significant enhancement in the fusion rate [41,42].

The observed resonant structure in ^{12}C+^{12}C elastic scattering [35,43] and in the fusion cross-sections is often explained as molecular states in a two ^{12}C cluster system [44–46]. This interpretation suggests a certain uniqueness, since such pronounced resonant structures have not been observed so far in fusion systems involving other light ion isotopes [47–49]. This may be due to the uniquely low number of open channels in the ^{12}C+^{12}C reaction [50]. This effect should be less pronounced in other fusion reactions such as ^{12}C+^{16}O and ^{16}O+^{16}O.[50]

The appearance of resonant structures in the ^{12}C+^{12}C fusion cross-sections poses a serious challenge for deriving a reliable reaction rate. The resonance parameters, such as partial widths and spin parity values, are not known and require additional analysis to identify the physical nature of the resonance feature.

As a consequence, the predictions for the aforementioned carbon burning environments carry a large uncertainty. Microscopic multichannel calculations are at the present state not accurate enough to predict the resonant fusion cross sections at the relevant stellar energies for these environments [15]. So far, model predictions rely on simple potential models or other parameterizations to extrapolate the cross sections toward the stellar energy range (i.e. [51,52]).

In-beam γ spectroscopy measurements seemed to support the suggested enhancement with fusion under the barrier [53–55] and appeared to require a modification of Coulomb transmission functions for the fusion process [56]. The early effort in γ spectroscopy was followed by extensive measurements of proton and alpha particle decay channels that provided more information about the possibility of resonances associated with the ^{24}Mg compound nucleus [40].

Renewed efforts were made to search for low-energy resonances, but the results were challenged by background contributions [57–59], while in other experimental efforts the resonance features were smeared out by thick-target effects due to the substantial energy loss in the target, providing only averaged cross-sectional information for the observed reaction channels [7,60,61]. Correcting the averaged cross section for target thickness effects revealed a more pronounced resonance structure over the lower energy range, as observed in multiple particle and gamma decay channels, confirming that the lower energy range was characterized by resonances [5,6].

The difficulties in reliable prediction for the low-energy extrapolation of ^{12}C+^{12}C and other light-ion fusion reactions were further complicated by the suggestion that the low-energy cross section might actually be reduced due to a hindrance term associated with the incompressibility of nuclear matter [4]. Within this concept, the hindrance was an effect that was anticipated for the case of the fusion of two more massive nuclei [62], an idea that developed from detailed experimental evidence observed in the fusion processes of heavier isotopes [63–66]. An alternative explanation to the hindrance term is the deformation or clusterization of reaction partners [64,67,68], although there is evidence that such an effect exists in medium-mass systems toward very low sub-Coulomb energies. However, the extent of the effect for light ion fusion systems such as ^{12}C+^{12}C or ^{16}O+^{16}O has not yet been experimentally verified [5] because the critical energy range has not been reached by direct measurements. Beyond phenomenological models, such as those summarized in Hagino and Takigawa [69] and Jiang et al. [65], the hindrance effect has also not been fully theoretically confirmed, as demonstrated by the time-dependent Hartree-Fock approach [68], or by a combination of mean field and cluster model [70,71]. Better microscopic techniques are necessary for a full theoretical evaluation.

Several experimental techniques have been developed and applied in direct measurements of the ^{12}C+^{12}C reaction towards lower energies. In the astrophysically important energy range, there are three main particle channels emitting neutron, proton, or alpha, respectively. These can populate the ground state or excited states in the residual nucleus that subsequently decay by gamma emission to the ground state. The contribution of neutron channels is typically a few percent or less [72], so experimental effort has been concentrated on measurements of the proton and alpha decay channels. Single direct measurements detect charged particles [40,58,61,73] or gamma radiation [47,54,55,57,60,74,75]. In particular, the γ-only approach typically measures the gamma transitions from the first excited states of ^{23}Na at 440 keV and ^{20}Ne at 1634 keV, including direct populations through the p_1 and α_1 channels to the respective first excited states of the final nucleus and cascades from higher excited levels. The downside of this approach is that it does not account for contributions from ground-state populations and can be severely affected by sodium contamination at the target. The particle-only approach, on the other hand, can obtain ground-state contributions. However, it will miss contributions from the higher excited levels because of particle detection limits. A further handicap is the beam-induced background from impurities of hydrogen and deuterium in the target. In recent years, a new approach using the particle-gamma coincidence technique between proton or alpha particle emission and subsequent γ transitions has been developed and has been applied in several experiments [5–7,76]. It

largely reduces the background issues that have handicapped the singles measurements, although contributions from the ground state an levels at higher-excitation energies will be be missed. The most important channels for coincidence measurements are the p_1 transition followed by the 440 keV γ transition to the ground state) as well as the α_1 transition with subsequent ground state decay via the 1634 keV γ transition).

The above studies can also be re-categorized into the so-called thin or thick target approaches. The thick target approach typically stops the beams in the carbon target and directly measures the reaction yield for an infinitely thick target. The thin target approach uses transmission-type targets and can directly measure cross sections. For this kind of approach, the energy loss of the beam should be small relative to the expected width of the resonance structures (typically 100–200 keV in the center of mass frame) [6]. However, the reaction yields extracted in the previous works (e.g. [40,76]) have to be averaged over the large energy loss range of a few hundred keV in the target. For example, a 50 (or 70) μg/cm^2 thick carbon target, as used in [40,76], results in an energy loss of about 360 (or 500) keV for 6 MeV carbon beams. In addition, there is some uncertainty in the thickness of the target, due to the carbon build-up on the targets during ^{12}C beam bombardment [60]. This can easily impact the large energy loss of the impinging ^{12}C particles at low energies.

The hindrance factor [4] is predicted to have a significant impact on the low-energy extrapolation of the cross section, as several stellar model simulations demonstrate [16,77–79]. It predicts the reduction of the S^* factor of the reaction towards lower energies as shown in fig 2. Although it might reduce the overall transmission probability through the Coulomb barrier, it needs to be considered in the context of possible, yet presently undetected, low-energy resonances. Due to the extremely and rapidly declining cross section, it seems unlikely that the direct experimental approach will reach these low energies in the near future, despite the new efforts of the experimental community [80,81]. However, new interesting results based on indirect reaction studies using the approach [82–88] have been presented, which seem to provide the first look at the resonance pattern in the low-energy fusion range. An analysis of the THM data including the possibility of the hindrance feature as suggested in [4] can be instructive.

3 Recent reaction studies in ^{12}C+^{12}C

The ^{12}C+^{12}C system fuses into a ^{24}Mg compound nucleus with an excitation energy of 13.934 MeV + $E_{c.m.}$. The compound nucleus decays by emitting α, p and n (see Fig. 1). The α transfer reaction is also possible to produce ^{8}Be+^{16}O. Following particle emissions, the excited residual nuclei decay to their ground states by γ-emission.

The previous efforts of direct experimental studies are assessed in [60] in a combined display of the total ^{12}C+^{12}C excitation function based on particle- [38,40,73] and gamma measurements [47,54,55,74,90]. Such studies require a precise knowledge of beam energy and impurities in the beam or the target such as ^{13}C or deuterium [59,91]. The main limitations for accurate measurements of subbarrier cross sections are the normalization method and possible carbon build-up on the target [92,93]. Another concern is the accurate determination of the effective beam energy over the energy loss of the impinging ^{12}C particles. In the ^{12}C+^{12}C fusion only resonance states with natural spin and parity are expected to be populated. Angular distribution measurements would be necessary for the spin assignment [40,73,94], but such studies will be handicapped by the low count rate at low energies.

The focus of more recent studies was on further approaching the astrophysics energy range of interest within $E_{\mathrm{c.m.}} = 1-3$ MeV. This was eventually attained by Spillane et al. [57]. In this experiment, gamma-ray detectors were utilized to map the characteristic gamma yield for an infinitely thick ^{12}C target. The yields of the energy steps between 12 and 25 keV were subtracted allowing for identifying a narrow resonance at the lowest energy reached so far in direct measurements at $E_{\mathrm{c.m.}} = 2.14$ MeV [5,7,58]. The studies and extrapolations are summarized in Fig. 2 showing the modified S-factor S^* below the Coulomb barrier at $E_{\mathrm{c.m.}} = 6.6$ MeV. The S^*-factor removes the exponential drop from tunneling through the repulsive Coulomb potential, correcting also for an extended size of the interacting nuclei [95]. It is defined as

$$S^* = \sigma E \exp(2\pi\eta + gE), \tag{1}$$

with the Sommerfeld parameter $\eta = Z_1 Z_2 e/\hbar v$ and $g = 1.22\sqrt{\mu R^3/Z_1 Z_2}$ the form factor for ^{12}C+^{12}C collisions [38]. The constants $Z_{1,2}$ are the charges of the nuclei, while R and μ denote the square-well radius and the reduced mass of the system.

Data from particle and gamma spectroscopy measurements are presented in Fig. 2 reaching far below the Coulomb barrier at $E_{\mathrm{c.m.}} = 6.6$ MeV. Note that the displayed S^*-factor translates into a decline in cross section of more than 8 orders of magnitude. The data by Spillane et al. [57] in Fig. 2 reproduce the oscillations in the cross section observed in [50]. The uncertainty increases drastically towards the deep sub-Coulomb barrier energy regime, where the cross sections are ceasing in the femto-barn range with the S-factor showing an uncertainty range of more than an order of magnitude between the extrapolations in the astrophysics region of interest.

Such experiments are typically conducted with beam intensities of several micro-amps on target over the course of multiple weeks. This requires durable measurement equip-

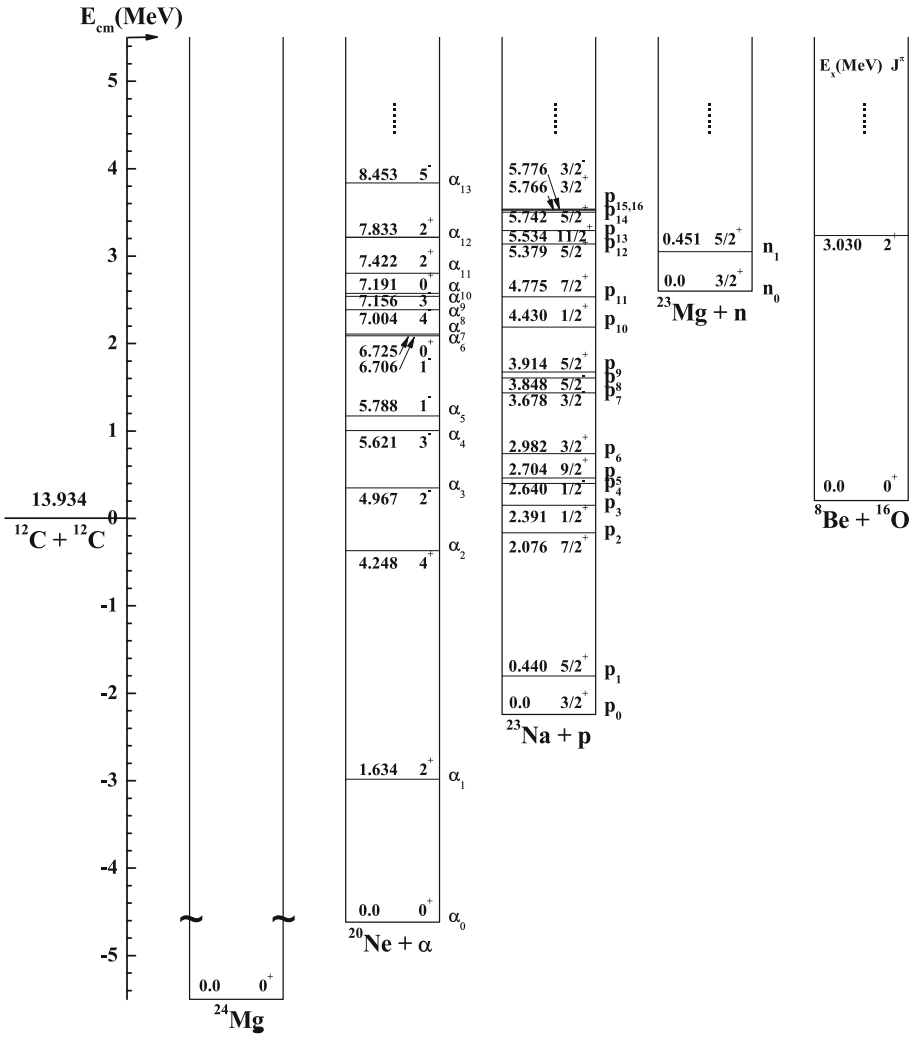

Fig. 1 Energy-level diagram for the $^{12}C+^{12}C$ system, showing the different particle decay channels of the respective compound states. Reprinted with permission from Ref.[89]

ment for reliable and stable data acquisition, as well as efficient background suppression for cross sections of the order of 100 pbarn and below. In order to achieve higher background suppression, the gamma-particle coincidence approach proposed by Jiang et al. [96] combines the detection of emitted light charged particles and gammas from the de-excitation of the daughter nuclei for exclusive measurements. Direct transitions to the ground state cannot be detected. This requires comparing the coincidence measurements with the results of direct particle spectroscopy studies [40,61].

The first coincidence experiment was carried out at ATLAS at the Argonne National Laboratory, United States, by combining the Gammasphere array with annular silicon detectors, which cover forward and backward angles in close geometry around a self-supporting target foil [76]. The efficient background reduction during measurements down to 2.7 MeV out-weights the lower total detection efficiency of approximately 9% for $E_\gamma = 440$ keV and 7% for $E_\gamma = 1635$ keV and S-factors with significantly improved accuracy were derived (see Table I and Fig. 4 in Ref. [76]). Data were analyzed and fitted with the hindrance parameterization [2,62] identifying a broad S-factor maximum around $E_{\text{c.m.}} = 3.5-4.0$ MeV. The extrapolation of such trends into the Gamow range would have drastic consequences on stellar burning and nucleosynthesis, as pointed out by Gasques et al. [77].

So far, two more experiments with coincidence background suppression technique were performed, at the Andromède accelerator at IJCLab Orsay, France, and at the 5U pelletron accelerator at the University of Notre Dame, United States.

The STELLA (STELlar LAboratory) mobile experimental station [97,98] at Andromède uses 36 $LaBr_3$(Ce) detectors from UK-FATIMA [99,100] and high-granularity annular silicon strip detector placed around a large thin ($30-50$ μg/cm^2) self-supporting target. The ^{12}C enriched carbon foil spans over a frame (diameter 6 cm) and spins with up to 1000 rpm. The beam hits the target at an outer spot so that the rotation creates a trajectory on the foil and heat from straggling of the beam in the target dissipates *via* radi-

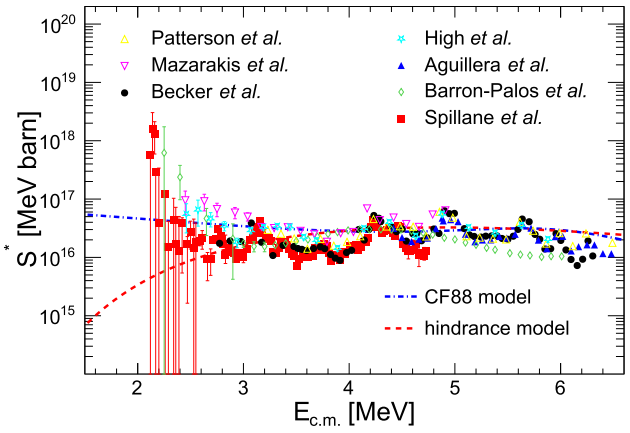

Fig. 2 Carbon fusion S-factor S^* from particle [38,40,73] and gamma measurements [55,57,60,75] (left and right legend, respectively) as well as extrapolation models proposed by Fowler et al. (CF88 [51]) and Jiang et al. (hindrance [2])

ation when the material is rotated off the beam spot position. Repeated thickness determination before and after irradiation serves accurate cross-section normalization (see Ref. [101] for details). The angular opening of the particle detector strips of the order of 10 mrad allows for the determination of exclusive angular differential cross sections of evaporation alphas and protons. These angular distributions can be decomposed into Legendre polynomials, that are used to accurately normalize the measurements [102] and to determine the spin parity of resonance structures of the excitation function [40,73,94]. The setup allows furthermore for gamma-particle timing gates of about 10 ns [101] offering exceptional background suppression. This is exemplified in Fig. 3 for a beam energy of $E_{\mathrm{c.m.}} = 3.8$ MeV for the particle detector spectra without gamma-ray coincidence (left) and in coincidence with a 1.634 MeV gamma ray associated to the α_1 transition to the first excited state in ^{20}Ne (right).

The coincidence condition virtually removes all contamination in the spectrum including a strong contribution from the $d(^{12}\mathrm{C}, p)^{13}\mathrm{C}$ reaction. The non-coincident background falls outside the characteristic timing gates of each reaction channel, determined by gating well beyond the characteristic timing offsets [103]. In the regime of low counts statistics, the background is subtracted from the measurement using a framework of unified classical confidence belts [104] avoiding negative counts and hence guaranteeing accurate confidence intervals. The stability of the selection gates during extended data acquisition runs is monitored *via* the non-gated energy (background) spectra of the gamma-ray detectors [105], repeated α-source runs (silicon detectors) and reference synchronization systems between both acquisition systems. The measurements down to $E_{\mathrm{c.m.}} = 2.16$ MeV with largely improved uncertainty at the lowest energies confirm the resonant structure reported in Ref. [57] and are in fair agreement with the hindrance trend [76] in the intermediate energy regime $E_{\mathrm{c.m.}} = 2.5 - 4.0$ MeV.

The coincidence setup hosted at the University of Notre Dame [5,6] employed the Silicon-detector Array at Notre Dame (SAND) [106] in combination with a HPGe detector at the back of a thick HOPG (Highly Ordered Pyrolytic Graphite) carbon target. The superior purity of HOPG compared to natural graphite efficiently reduces the background related to hydrogen, deuterium, and ^{23}Na, the latter being vulnerable to scattered beams. For example, an early test [107] showed that HOPG targets can reduce impurity of heavy elements that can cause backscattering of the beams by two orders of magnitude. Comparison with previous measurements from other experiments shows that the background effect is negligible at higher beam energy, but may be significant at lower energies. The segmented silicon detectors are optimized to the target geometry with the lampshade configuration of SAND in addition to an annular detector, offering

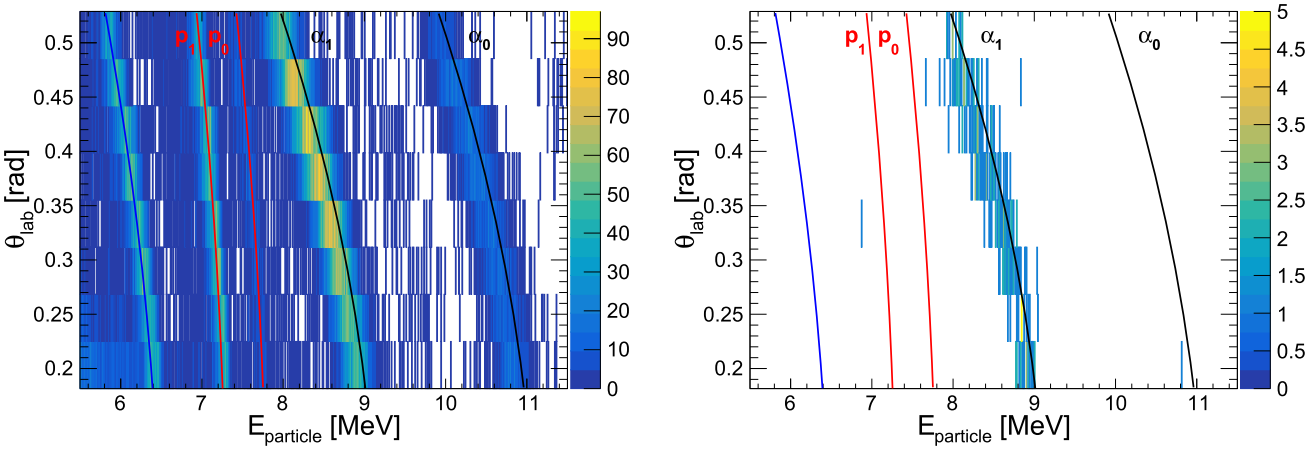

Fig. 3 A STELLA charged particle detector spectrum at the beam energy $E_{\mathrm{c.m.}} = 3.8$ MeV. The contamination in the non gated spectrum (left) is completely removed with the coincident 1.634 MeV gamma ray associated to the α_1 transition (right)

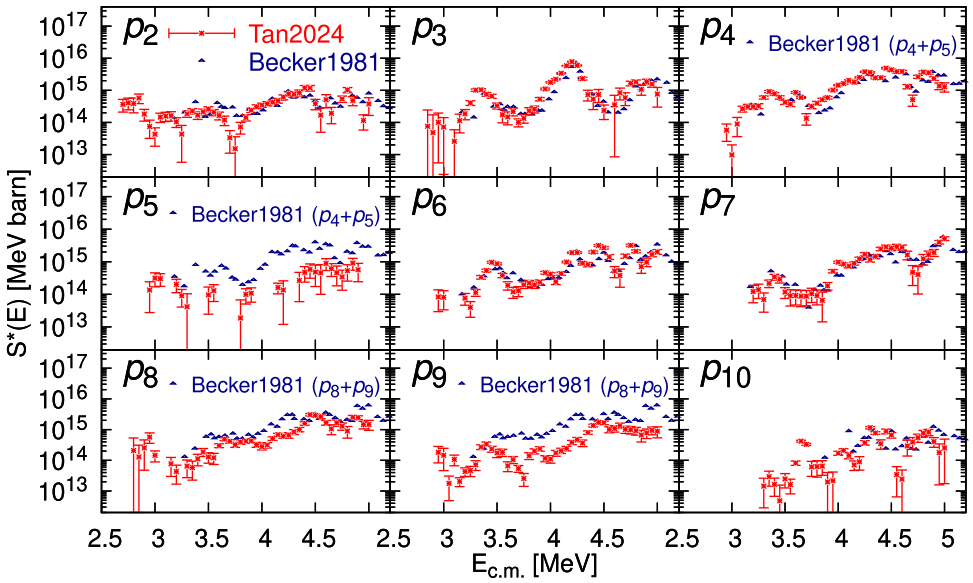

Fig. 4 The p_2-p_{10} S-factors from two data sets [6,40] are shown and compared

a vast angular coverage in the backward direction (102° to 170° in the laboratory frame). Using the particle-γ coincidence technique, partial cross sections of the α_1 and p_1-p_{10} channels were determined over a wider energy range through a differential thick target analysis [108]. In particular, the thick target yields were measured in steps of 50 keV resulting in an improved energy resolution as compared to conventional approaches. Such a fine energy resolution reveals several pronounced resonance-like structures in the energy range of $E_{\mathrm{c.m.}} = 2.6 - 5.0$ MeV in reported S-factor data, which were observed in all measured proton and alpha channels. These observed structures largely overlap with the results from Becker et al. [40] especially at higher energies. The S-factor results are consistent with previous measurements at higher energies but tend to be lower than previous results at lower energies, due to the cleanness of the experimental approach or possible energy-dependent efficiency issues as discussed below. During coincidence measurements, the background is estimated outside the energy selection gates of gammas and particles, and conservative upper limits of the α_1 and p_1 S-factors for the proposed narrow resonant structure at $E_{\mathrm{c.m.}} = 2.2$ MeV were obtained, well below the results from Ref. [57].

New Notre Dame results [6] show that partial cross sections of the proton emission channels (p_1-p_{10}), as shown in Figs. 4 and 5, are in good agreement with previous measurements at energies where individual channels are resolved. The differential thick target approach that is robust for the proton channels, unfortunately, is problematic causing significant yield reduction for the α_1 channel due to target deterioration with beam accumulation (see details in Ref. [6]). After corrections of the yield reduction effect with an improved α_1 analysis, the α_1 S-factor, as shown in Fig. 6, is much higher than that of the p_1 channel at energies around 3 MeV and

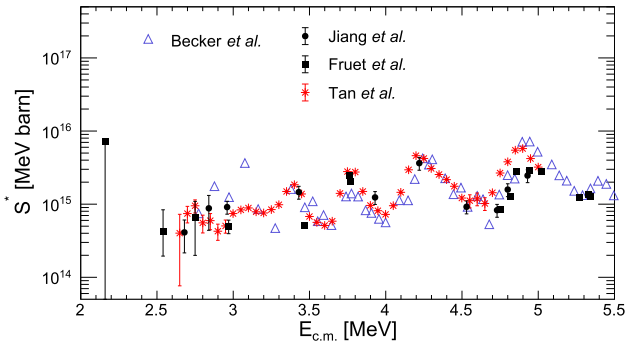

Fig. 5 The modified p_1 S-factor S^* data from coincidence measurements [6,7,76] are compared to Becker et al. [40]

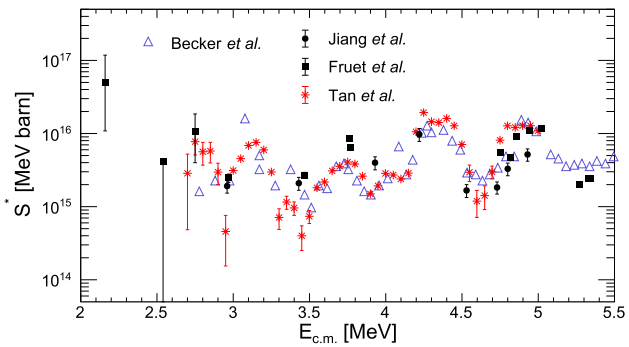

Fig. 6 The modified α_1 S-factor S^* data from coincidence measurements [6,7,76] are compared to Becker et al. [40]

below. To continue measurements at even lower energies using this approach, however, new development in target technology (e.g., more robust diamond targets than HOPG) will be necessary.

At the lowest energies reached in direct measurements, the cross sections are of the order of 100 pb or below resulting

in few-count statistics. The angular differential cross section was taken to be isotropic. The systematic uncertainty of the partial cross sections is setup-dependent and was estimated to be about 20% for p_1 and 60% for α_1 in extreme cases for a specific setup [5]. The focus of coincidence experiments in this energy regime was on the α_1 and p_1 exit channels. For total S-factors, the results were then normalized to the decay channel branching from Becker et al. [40] averaged over all higher energy measurements [5,76,98]. In a more recent compilation [89], the branching ratio was assessed with extrapolations based on a statistical treatment of the ^{24}Mg compound nucleus. The extracted ratios of partial cross sections follow experimental data with smooth extrapolation towards lower energies justifying the above assumptions.

A new direct measurement of proton and alpha particles emitted in the fusion process was initiated at the CIRCE laboratory [58]. Particle identification was achieved using ΔE-E_{rest} silicon telescopes. This prevented the possibility of identifying the alpha particles emitted in the reaction since they could not pass the ΔE detector. To be able to observe also the alpha channel, a detector tailored towards the identification of low energy charged particles was developed [109].

The detector system, named GASTLY (GAs-Silicon Two-Layer sYstem), consists of a ΔE-E_{rest} telescope that uses an ionization chamber as the ΔE energy loss detector and a large area Si detector (58.0 x 58.0 mm^2 active area, 300 μ m thick) to determine E_{rest}. The entrance window to the detector is a 2.5 μm thick Havar foil. All of the materials were selected to have very good resistance and stability in withstanding the high temperatures reached by the graphite target under intense beam. The ion chamber is operated with CF4 gas, in order to minimize hydrogen and therefore deuterium contamination in the residual vacuum of the reaction chamber.

The full detection setup consists of an array of seven GASTLY modules, placed in close geometry to the target, in this case at 52 mm distance, at backward angles with respect to beam direction. In this configuration, each of the close detector modules covers a solid angle of about 19°x19°. A detailed study of the deuterium content in graphite targets was conducted [59], in order to minimize the possible influence of protons produced in $d(^{12}\text{C}, p)^{13}\text{N}$ at the lowest measurement energies through the double step process identified in [110]. Cross-section measurements were made using the thick target approach, spanning a center-of-mass energy range of 2.4 to 4.4 MeV for protons and 2.9 to 4.4 MeV for alpha particles, with energy increments of approximately 25 keV. At energies lower than 2.9 MeV the alpha particles could not be separated anymore from the background. Figure 7 shows the ΔE-E_{rest} spectrum of the detector placed at 121° with respect to beam direction, acquired at the center of mass beam energy of $E_{\text{c.m.}}$ = 4.36 MeV.

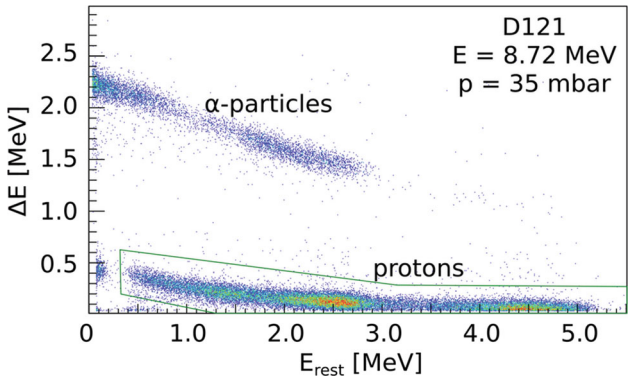

Fig. 7 Sample ΔE-E_{rest} matrix showing the α particles and protons loci. This spectrum was acquired at E_{lab} = 8.72 MeV [61]. The signals for the p_0 and p_1 transitions are located around 5 MeV and the transitions for p_2 to p_6 can be seen around 2 MeV. The background below 2 MeV is dominated by deuterium induced processes

The spectrum demonstrates excellent separation of the proton and alpha loci. Analysis of the energy spectra of the particles in the proton loci allowed identification of the groups p_0 to p_6 at all energies. However, some groups could not be quantified at the energies at which the remaining background signal from the reaction $d(^{12}\text{C}, p)^{13}\text{N}$ overlapped. Due to the larger energy loss in the entrance window, only the α_0 and α_1 groups could be effectively detected and quantified.

It should be noted that, in addition to [40], only [58], directly measured the p_0 channel, with [61] adding the information to the decay channel α_0. The α_0 cross section measured by [61] is lower than previous measurements [40,73]. This might suggest that the α transitions to higher excited states in ^{20}Ne dominate the cross section. Since these are the only two measurements probing the α_0 channel it is necessary to invest in more detailed studies of this channel towards lower energies.

Figure 8 shows the comparison between the data from direct studies based on γ spectroscopy, γ particle coincidence spectroscopy and particle spectroscopy presenting both the excitation curve for the total $^{12}\text{C}(^{12}C, \alpha)^{20}\text{Ne}$ and the $^{12}\text{C}(^{12}C, p)^{23}\text{Na}$ reaction channel. The $^{12}\text{C}(^{12}C, \alpha)^{20}\text{Ne}$ data by [61] seem systematically lower because they rely on a direct measurement of theb α_0 channel, while the other data sets are normalized to [40].

The $^{12}\text{C}(^{12}\text{C}, n)^{23}\text{Mg}$ reaction channel is a weak channel, in comparison to the α and p channels discussed in the above. This channel closes at its threshold energy of $E_{c.m.}$=2.6 MeV and therefore will only contribute to the fusion process at high temperature conditions. The $^{12}\text{C}(^{12}\text{C}, n)^{23}\text{Mg}$ reaction was first measured by Patterson et al. [38] and Dayras et al. [111], respectively, above the astrophysical energy range through the detection of β- or γ-rays from the decay of

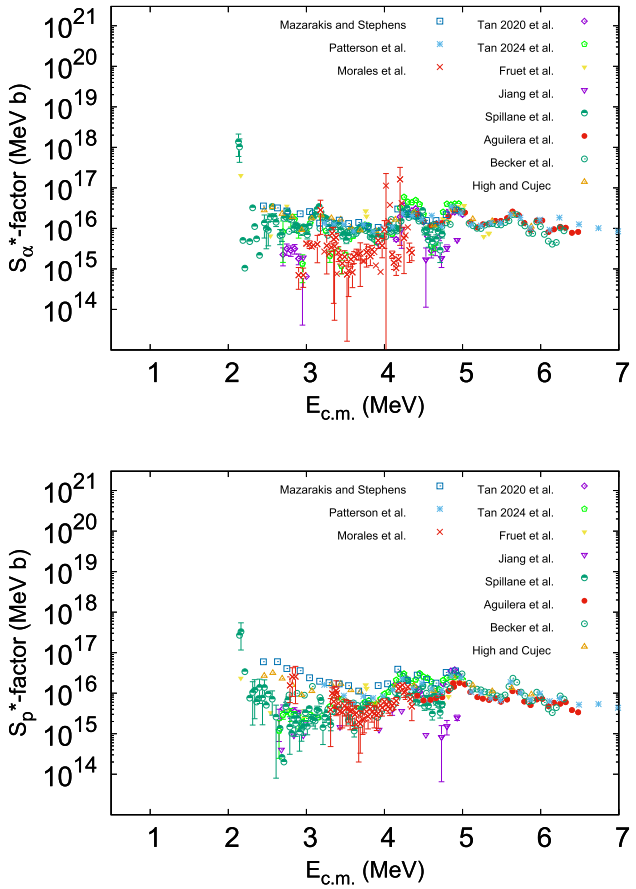

Fig. 8 Results of the direct measurements of the α-channel (upper panel) and p-channel (lower panel) contributing to the modified astrophysical S-factor for ^{12}C+^{12}C

^{23}Mg. Bucher et al. extended direct measurements down to $E_{\text{c.m.}} = 2.9$ MeV by counting neutrons using a ^{3}He detector array. The primary source of beam-induced neutron background arose from the ^{13}C(^{12}C, n)^{24}Mg reaction. The S-factor in the unmeasured energy range down to the threshold energy $E_{\text{c.m.}} = 2.6$ MeV was obtained with an extrapolation based on experimental data from the mirror reaction ^{12}C(^{12}C, p)^{23}Na and a statistical model calculation. At typical carbon shell-burning temperatures ($T_9 \approx 1.1-1.3$), the current reaction rate uncertainty is less than 40%. This uncertainty is further reduced to 20% at $T_9 \approx 1.9-2.1$, relevant for explosive carbon burning[72]. Future measurement with better technique is needed to further improve the accuracy.

4 Proposed reaction studies in ^{12}C+^{12}C

To expand on the presently existing results, it is crucial to have new direct experimental data towards lower energies to explore the resonant structures proposed on the basis of the data obtained by the Trojan Horse Method (THM) [3]. Such studies can be performed by detecting the emitted charge particles as a function of energy [40,61] or also by detecting the γ-rays generated by the decay of the ^{20}Ne and ^{23}Na excited states [6,98,112].

Charged particle spectroscopy has the advantage that the total fusion cross section can be measured. However, due to the very low energies involved, unambiguous identification of the reaction products is difficult, especially with low counting statistics. In contrast, γ-ray spectroscopy is rather straightforward but is blind to direct transitions to the ground states of the residual nuclei.

Due to 1400 m of rock overlying the experimental halls, the Italian INFN-Laboratori Nazionali del Gran Sasso (LNGS) is the ideal location for a γ-ray detection experiment. Since more the 30 years Laboratory for Underground Nuclear Astrophysics (LUNA) collaboration is active at LNGS to expand cross section measurements toward the Gamow range of stellar burning [113–118], using the LUNA400 keV accelerator. Since 2023 a 3.5 MV accelerator has been installed and is operated as Bellotti Ion Beam Facility at the LNGS [119]. The Bellotti IBF consists of a single ended machine by High Voltage Engineering Europa (HVEE) equipped with a specially designed ECR source tailored towards applications in Nuclear Astrophysics research, which can deliver an intense C beam. To our knowledge the machine provides one of the most intense Carbon beams available worldwide in this energy range [119,120].

The LUNA Collaboration plans to measure the ^{12}C+^{12}C fusion cross section at the Bellotti IBF, taking advantage of the intense C beam at the underground location. A dedicated γ-ray detection system, able to identify a few reactions per day, is currently under construction, promising a direct detection of the ^{12}C+^{12}C cross section below E = 2 MeV. The γ-ray spectroscopy needs to be performed with a detector that combines the best resolution to the highest possible efficiency. The most intense transitions to be detected at low energy correspond to the first excited states of ^{20}Ne and ^{23}Na, E_γ = 1634 keV and E_γ = 440 keV respectively, therefore, at energies lower than E_{cm}=2.5 MeV only these transitions can be observed.

The measurement reaching the lowest energy has been performed at the 4 MV Dynamitron Tandem accelerator of the Ruhr-Universität Bochum [57] using a high-purity germanium (HPGe) detector in close geometry surrounded by a 15 cm thick lead shield. The hydrogen contamination in the target became negligible by heating up the target [57]. The data do not extend towards low energies because of the too high level of environmental background.

The ^{12}C+^{12}C fusion reactions are an excellent case to be measured with γ-ray spectroscopy exploiting the low background conditions at the 3.5 MV underground accelerator at LNGS, where the cosmogenic background, including the muon-induced flux of γ-rays and neutrons, is strongly

reduced. The low muon flux and the consequent reduction of muon-induced secondary radiation in the heavy massive shielding surrounding the detector allow reducing also the radiogenic γ-ray background below 2.6 MeV to a level which cannot be reached above ground. Thus, the underground site provides ideal conditions for the detection of high-energy γ rays, as well as low-energy ones.

LUNA is developing a thick modular lead shielding, similar to [121] with a thickness of 25 cm. An additional reduction of about one order of magnitude in the low energy γ ray background below 2 MeV is possible by flushing the detector's surroundings with clean nitrogen [122] reducing radon background as summarized in [123]. This yields a total background reduction of more than 4 orders of magnitude [57] in the energy window around the energies of interest (440 keV and 1634 keV) as shown in fig 9.

The design of the γ-ray detection system is driven mainly by the goal of detecting the 440 keV and 1634 keV transitions with high sensitivity, i.e. a large full-energy detection efficiency with the lowest possible background in the energy region of interest. A good energy resolution of the detector allows smaller regions of interest, reducing the susceptibility to nearby backgrounds. To achieve design goals, a hybrid approach to γ-ray detection will be developed, involving an HPGe detector surrounded by a number of large-volume NaI(Tl) scintillation detectors. The scintillators surrounding the HPGe detector will actively shield this detector from environmental background radiation and will improve its peak-to-total ratio, suppressing low-energy background events caused by Compton scattering of high-energy γ rays, thus further enhancing the sensitivity for detection of low-energy γ rays.

5 Indirect methods in probing the compound structure of ^{24}Mg

The appearance of the pronounced resonant structures in the ^{12}C+^{12}C fusion cross-sections at astrophysical energies poses a serious challenge to derive a reliable reaction rate without knowing the nature and strength of these configurations as discussed earlier. Complementary to the direct measurements of the resonance states several indirect methods have been pursued to explore the nature of such states by probing the excitation range in ^{24}Mg, either by inelastic scattering techniques, by high-energy direct nuclear reaction studies or by high-energy transfer techniques in the Trojan Horse approach.

In inelastic scattering experiments with an alpha beam on ^{24}Mg [124,125], 0^+ resonances near the ^{12}C+^{12}C reaction threshold were identified [126] as di-carbon cluster states in ^{24}Mg [127] by detecting the decay pattern of the compound nucleus. It was furthermore suggested that the possible involvement of these states during stellar carbon fusion could change the reaction rate by up to an order of magnitude compared to standard extrapolation [126] possibly establishing an effective nucleosynthesis mechanism due to the contribution of pronounced low-energy 0^+ s-wave resonances. However, this claim is challenged by compound reaction studies of ^{20}Ne(α, α_0) [128] and ^{20}Ne(α, $\alpha_{1,2,3}$) [129], which did not identify 0^+ states in the predicted energy range.

Another attempt, following a similar route as suggested by [130], to investigate the excitation range in ^{24}Mg via ^{23}Na(p, $p_{0,1}$) and ^{23}Na(p, $\alpha_{0,1}$) is being pursued at the University of Notre Dame via the time reversed ^{20}Ne(α, p)^{23}Na reaction using a recirculating gas target system. The reaction will allow the parallel mapping of the alpha cluster and single particle strength distribution in ^{24}Mg and explore the correlation to the resonance structures observed by THM.

Although all these indirect reactions provide important surrogate information about the level density and the level structure near the ^{12}C+^{12}C fusion threshold, the Trojan Horse approach suggests a direct link to the reaction mechanism of the ^{12}C+^{12}C fusion reaction without being handicapped by the Coulomb barrier. The THM is an indirect technique aimed at determining the astrophysical S(E) factor for rearrangement reactions involving charged particles [87,88,131]. The primary concept involves measuring the cross section of a THM reaction where three particles characterize the exit channel:

$$A + a \rightarrow C + c + s, \tag{2}$$

to deduce the cross section of the process of astrophysical relevance (in the following referred to as NPA=Nuclear Astrophysics Process):

$$A + x \rightarrow C + c. \tag{3}$$

This cross section is obtained without the need for extrapolation, under specific conditions, and by utilizing advanced nuclear reaction theory [88]. In a simplified explanation, assuming the imposition of quasi-free kinematics (QF) and a strong $x + s$ cluster structure for particle a, the interaction between x and A remains unaffected by the presence of s, which acts as a spectator. The QF kinematics is enforced by selecting small $x - s$ relative momenta, ensuring that the $x - s$ relative distances are greater than the radius of the nuclear interaction. By selecting a beam energy in the THM reaction 2 that exceeds the Coulomb barrier, the influence of the Coulomb penetration factor is mitigated, allowing access to relative energies $x - A$ down to zero, thus covering the energy range of astrophysical interest. An additional advantage of this method is that the derived cross section of NAP remains unaffected by electron screening, allowing direct access to the cross section of the bare nuclei. The application of nuclear reaction theory is essential to establish the

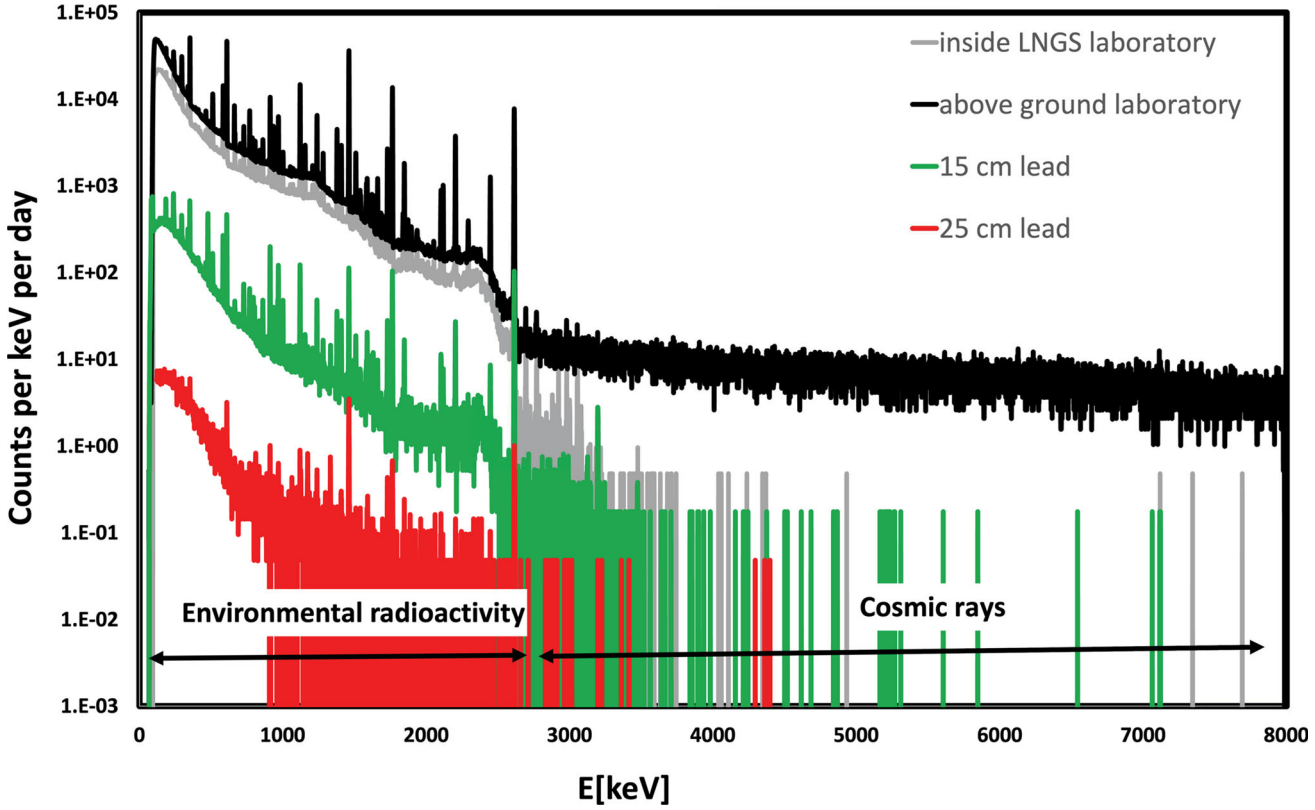

Fig. 9 Typical γ-ray background measured with a HPGe detector in a surface laboratory (black line), compared with one acquired underground without lead shielding (gray line), with 15 cm of lead around the detector (green line) and 25 cm (red line)

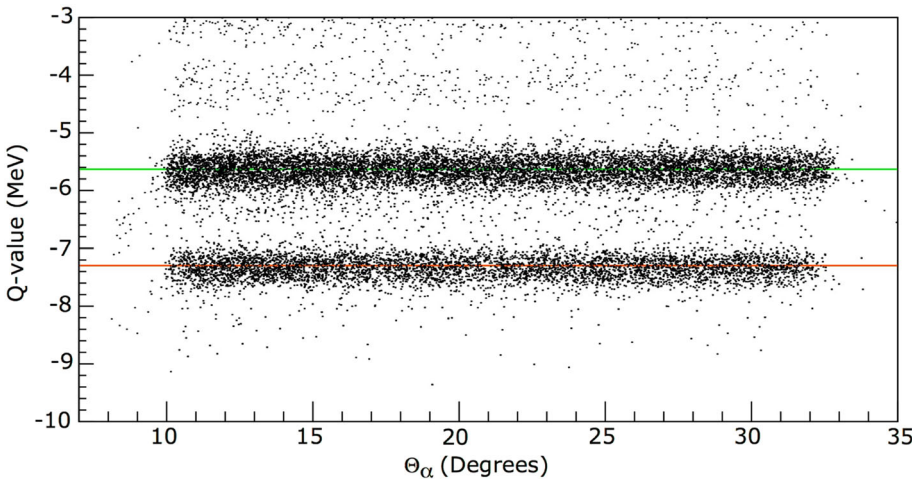

Fig. 10 Q-value as a function of the α detection angle (θ_α) for the ^{12}C(^{14}N,α^{20}Ne)^{2}H reaction. Green and red solid lines highlight the contributions of ^{20}Ne ground and first excited states, respectively

connection between the cross sections of the THM and NAP reactions.

Recently, various efforts have been made to improve and generalize the theoretical framework connecting the two cross sections and to evaluate the systematic uncertainty introduced by model dependence as discussed in [87,88,131]. These reviews present theoretical advances in the framework of classical reaction theory and assumptions on wave functions at near-threshold energies. In the case of reactions dominated by broad resonances, the use of the modified R-matrix approach [132,133] has made it possible to account for half-off-energy-shell and energy resolution effects, in the well-assessed R-matrix framework. Additional advantages were the possibility of performing a multichannel description of the reaction process (as in the ^{12}C+^{12}C fusion studies, see [3]) and including a DWBA-based description of the QF process, possibly leading to a normalization procedure that does not require the use of direct data [134]. In the

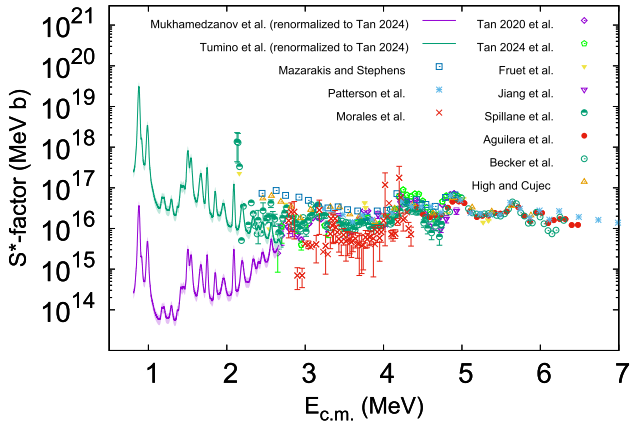

Fig. 11 Direct (symbols) and indirect THM (lines) measurements of the total, modified astrophysical S^*-factor for ^{12}C+^{12}C. The higher energy data show pronounced resonance structures, which differ in the strengths of the transition to the ground states and higher excited states. The difference between the two THM data sets in the low energy range is due to theoretical differences in the conversion of the direct THM data to $S^*(E)$ factors

case of reactions dominated by narrow resonances, a simplified approach [135] has been introduced to deduce resonance strengths directly from the cross section of reaction 2. By performing a multi-resonance normalization and thanks to the covariance in error propagation, systematic errors from normalization and theory are reduced to the percent level.

5.1 THM studies for ^{12}C+^{12}C

The fusion cross section of ^{12}C+^{12}C at astrophysical energies was deduced for both ^{12}C(^{12}C, α)^{20}Ne and ^{12}C(^{12}C,p)^{23}Na reactions channels using the Trojan Horse Method utilizing the ^{12}C(^{14}N, α ^{20}Ne)^{2}H and ^{12}C(^{14}N,p^{23}Na)^{2}H three-body processes in quasi-free (QF) kinematics, with deuterium from ^{14}N acting as a spectator to the ^{12}C+^{12}C reactions [3]. This experiment was conducted at the INFN - Laboratori Nazionali del Sud in Catania, Italy. A beam of ^{14}N accelerated to 30 MeV by the SMP TANDEM was directed at a carbon target with a density of 100 μg/cm^2. The products of the two-body reactions (either α or p) were detected in coincidence with the spectator deuterium particle using silicon telescopes placed on both sides of the beam, covering optimized angular regions for the QF kinematics of the breakup process. Coincidence events were identified by gating in the two-dimensional plots ΔE-E to select d and $\alpha(p)$ loci. Kinematics was reconstructed under the assumption of undetected particles, either ^{20}Ne (for the α+d channel) or ^{23}Na (for the p+d channel). The Q value was analyzed as a function of a kinematic variable, such as energy or angle, with coincidence events expected to align horizontally at the predicted Q value. Figure 10 illustrates a typical spectrum for the reaction ^{12}C(^{14}N,α^{20}Ne)^{2}H, showing the Q-value as a function of the α detection angle. Two prominent horizontal loci indicate the ground and first excited states of ^{20}Ne, marked by green and red lines at -5.65 MeV and -7.28 MeV, respectively. This spectrum confirms the calibration quality and background free channel selection, leading to further analysis being focused on these events.

Further experimental details can be found in [3]. The dominance of the QF mechanism was supported by the close agreement, within 5%, between the experimental momentum distribution (in the 30–80 MeV/c range) and that derived from the Woods-Saxon potential of the ^{12}C-d bound state, with standard geometric parameters like r_0 = 1.25 fm, a = 0.65 fm, and V_0 = 54.428 MeV, adjusted to match the experimental ^{12}C-d binding energy in ^{14}N. Recently, a corresponding agreement with the theoretical momentum distribution calculated using the Distorted Wave Born Approximation (DWBA) was demonstrated within the 30–80 MeV/c experimental range. This significant finding will be detailed in a forthcoming publication.

Following the completion of various data analysis steps [3], the two-body cross section relevant to astrophysics was determined applying the Plane Wave Impulse Approximation (PWIA) for four channels: ^{20}Ne+α_0, ^{20}Ne+α_1, ^{23}Na+p_0, and ^{23}Na+p_1. A modified one-level, many-channel R-matrix analysis was performed, incorporating the ^{24}Mg states as documented in [3]. The convenience of PWIA stems from its straightforward connection to the three-body cross section, a connection guaranteed in the modified R-matrix approach by the presence of the same matrix elements in the total PWIA amplitudes as in the on-the-energy-shell binary reaction cross section (refer to eq. 3 of [3]). Based on the findings in [40] at center-of-mass energies $E_{\rm c.m.} \leq 3$ MeV and observations of decreasing penetration factors for specific states, the portion of the total fusion yield from α and p channels outside of $\alpha_{0,1}$ and $p_{0,1}$ was disregarded in the modified R-matrix analysis. The estimated errors at $E_{\rm c.m.}$ below 2 MeV were below 1% for the α channels and 2% for the p channels. The reduced widths of the THM based states were integrated into a standard R-matrix algorithm to determine the S(E) factors for the four reaction channels.

The results are illustrated in fig 11, showing the total modified $S^*(E)$ factor determined in the past direct and indirect experimental campaigns. The data above 3 MeV represent the results of the direct reaction studies based on different experimental techniques as also shown in fig 8, while the energy range below 3 MeV shows the THM result by [3] and the proposed rescaling by [136], normalized to the direct data of [6] as discussed in the following section.

6 Theoretical studies for ^{12}C+^{12}C

A theoretical Coulomb correction to the THM data, as detailed in [136], was proposed using a DWBA-based theory

without resonances. This reanalysis produced significantly lower values $S^*(E)$, with discrepancies extending up to four orders of magnitude compared to earlier results. However, the authors perform a single resonance approximation, disregarding the presence of several ones [137], using a common zero-range DWBA cross section of the transfer reaction to determine the renormalization factor. Moreover, the convergence and numerical stability of calculations related to transfer to the continuum need careful scrutiny to avoid outcomes that are highly sensitive to the specifics of the model space. For example, theoretical calculations employing the Feynman path-integral method [138] yielded S-factor values that align well with the THM results. A recent study by Taniguchi and Kimura [139], which utilizes the generator coordinate model and incorporates full coupling between the entrance and exit channels of the ^{24}Mg compound nucleus, suggests the formation of notable ^{12}C+^{12}C molecular states. These states fragment into multiple narrower resonances, which are suggested to correspond predominantly to 0^+ and 2^+ spin parity considerations [139], due to channel coupling, consistent with the experimental spectrum indicating several low-energy states, as inferred from the THM data. However, the use of the R-matrix formalism to derive cross sections yields significantly lower results than those proposed by [3]. This finding is not definitive, as it does not account for non-resonant contributions and potential interference effects.

Accurate prediction of low-energy extrapolation of fusion reactions involving ^{12}C+^{12}C and other light ions is complicated by the potential "hindrance" effect, which may reduce the low-energy cross section. However, the impact of this effect in light ion fusion systems with $Q_{val} > 0$ remains unclear, particularly for reactions like ^{12,13}C+^{12,13}C and ^{16}O+^{16}O, which have not been experimentally verified [140]. Precisely, the results of [140] for the ^{12}C+^{13}C fusion dismiss the predicted maximum in the astrophysical S(E) factor suggested by the hindrance model but support a rising trend at lower energies. The hindrance effect lacks theoretical confirmation, as it is not observed in time-dependent Hartree-Fock (TDHF) calculations [141] or in the combination of mean field and cluster models [70]. In summary, the issue of theoretically reliable extrapolation remains unresolved. The nature of these low near-threshold energy states and any possible interference effects are still under investigation. A comprehensive exploration and comparison of various theoretical approaches and methodologies are essential for achieving a deeper understanding and establishing more reliable outcomes in this field.

Figure 12 shows different model calculations of the modified astrophysical S-factor for ^{12}C+^{12}C, such as those of the time-dependent wave-packet (TDWP) method, coupled-channel, neck model, microscopic hybrid alpha-cluster, the density-constrained time-dependent Hartree-Fock (DC-TDHF), and antisymmetrized molecular dynamics (AMD)

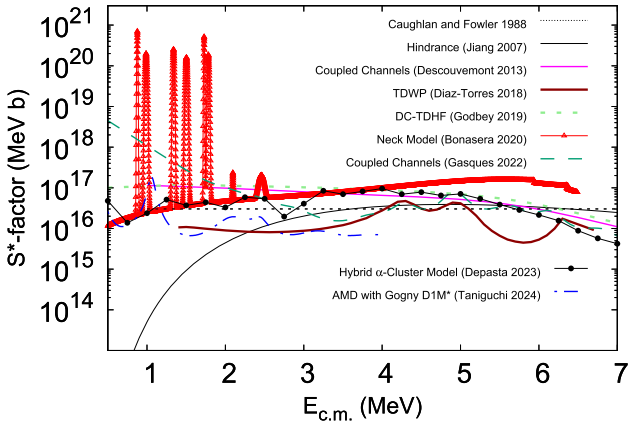

Fig. 12 Model predictions for the modified astrophysical S-factor for ^{12}C+^{12}C towards low energies

calculations. While most models describe the trend of experimental data (Fig. 8) at higher energies of ≈6 MeV rather well, large discrepancies exist at stellar energies of $E < 3$ MeV. The estimation by Caughlan and Fowler [51] (black-dotted line) assumes a constant S^*-factor, and a very strong suppression at stellar energies is predicted by the hindrance model (black-thin-solid line). The predictions of these different models differ by two orders of magnitude at the Gamow energy window ($E < 3$ MeV), which is centered at ≈1.5 MeV. In this energy region, most model calculations provide a smooth S^*-factor function, with the except of two. Namely, (i) the AMD model that microscopically treats compound nucleus resonances associated with different binary cluster configurations of ^{24}Mg (blue-dot-dashed line), and (ii) the neck model, which addresses a two-body potential model using the imaginary time method (red-triangles). In the AMD model [139], the microscopic compound-nucleus Hamiltonian matrix is diagonalized. The R-matrix method along with the Breit-Wigner formula for a single-resonance cross-section are then used for calculating the resonant S^*-factor, which is very sensitive to the energy density functionals [139]. In the neck model approach [138], the Bass potential strength increases at each 0^+ resonance observed in the THM data, adding resonance structures to a smooth S^*-function that notably disagrees with other predictions at near-barrier energies. In some cases the spin of the observed resonances was changed to 0^+ based on ref.[13] of [138]. The microscopic hybrid alpha-cluster calculations (black-solid circles) show fluctuations which may be due to numerical noise in the treatment of quantum tunneling with the imaginary time method [71]. DC-TDHF calculations [68] (light-green short-dashed line) using the Skyrme energy density functional, with the SLy4d parameter set, predict a S^*-factor function that is similar to the one from the coupled-channel calculations by Assunção and Descouvemont [142] (magenta-dot-dot-dashed line). The lat-

ter calculations include microscopic double-folding potentials using both the DDM3Y nucleon-nucleon interaction and transition densities from a triple-alpha cluster model. The coupled-channel calculations by Gasques et al. [143] (green-long-dashed line) predict a strong increase in the S^*-factor as the energy becomes smaller, reproducing the trend of the THM measurements [3]. This is because the set of parameters of the imaginary potential are chosen in such a way that they describe, on average, the THM measurements. These coupled-channel calculations use optical potentials based on the real Sao Paulo nuclear interaction, which is very attractive at short radii, and a weak angular-momentum dependent imaginary part, leading to resonant structures in the S^*-factor function at energies around the Coulomb barrier. Similar structures are yielded by the TDWP calculations [144] (dark-red solid line). However, discrepancies exist between the TDWP resonances and those in the coupled-channel calculations by Gasques et al. [143], which may be due to the absence of the ^{12}C intrinsic vibrations in the TDWP model [144] that only treats rotational modes of oblately deformed ^{12}C nuclei. The TDWP method directly solves the time-dependent Schrödinger equation with a multi-dimensional collective Hamiltonian, including the static quadrupole deformation and orientation of the ^{12}C nuclei [144,145]. The equator-equator orientation of oblately deformed ^{12}C nuclei facilitates their capture in the corresponding potential pocket due to the lowest Coulomb barrier among all the orientations. This potential pocket supports doorway molecular states that feed the fusion process of the pole-pole dinuclear configuration [145]. State-of-the-art, quantum dynamical microscopic calculations of ^{12}C + ^{12}C fusion have confirmed the crucial role of triaxial nuclear molecular configurations surviving the nuclear process in the formation of some resonant structures in the astrophysical S-factor [146]. Some of the resonant structures in the experimental data in Fig. 8, which are not yet explained, could be due to both compound nucleus resonances [146,147] and/or cluster effects in the nuclear molecule [139,148].

7 Astrophysical impact

In the following section, we discuss the implications of the ^{12}C + ^{12}C fusion rate in late evolution stellar environments at conditions where the reaction rate is less impacted by electron screening as at high-density conditions [149,150] anticipated for type Ia supernova, involving accreting or merging white dwarfs [19], or superbursts in the atmosphere of accreting neutron stars [22]. In the latter two cases, the reaction rate is expected to be enhanced by several orders of magnitude because of electron screening, with the nuclear physics aspects considered in the previous sections of this paper of lesser relevance.

The importance of a good knowledge of the cross section of the ^{12}C + ^{12}C nuclear reaction dates back to Becker and Iben [151] who were the first to name M_{up} the maximum mass that does not ignite C. They clearly stated that this critical mass depends (also) on the ^{12}C + ^{12}C nuclear reaction cross section (NRCS). Though early recognition of the importance of this NRCS, only in 2007 few theoretical tests were performed to check the role of this NRCS (taking advantage of a new, reduced, cross section obtained in the Hindrance scenario - HIN) on the evolution, in that case of the massive stars. More specifically, Gasquez et al. [77] showed the evolution of two massive stars (a 20 and a 60$M_\odot$) computed with a very detailed network for both the CF88 and the HIN cases. They found that the reduced rate lead to a significant increase of both the yields of ^{26}Al and ^{60}Fe, while the comparison between all other isotopic yields showed a maximum scatter of a factor of 4 only in few selected isotopes. Based on just these two masses, Gasquez et al. [77] argued, tentatively, that the new yield of the ^{26}Al would have alleviated the friction between theory and observations [152]). Later on, Bennett et al. [153] and Pignatari et al. [154] explored the consequences of both an increase and a decrease of this nuclear cross section on the evolution of a set of massive stars (15, 20, 25, 32 and 60$M_\odot$). None of these papers was based on a new measurement of this nuclear reaction, but either the cross section provided by CF88 was multiplied or divided by a fixed factor or a new cross section was derived by assuming the presence of a strong resonance at a center-of-mass energy of 1.5 MeV.This choice originated from a preliminary (at that time) particle spectroscopy experiment on ^{12}C + ^{12}C obtained at the CIRCE radioactive beam facility in Caserta/Napoli, Italy [155]. In these papers, they discuss the dependence of both physical and chemical evolution on the adopted ^{12}C+^{12}C NRCS. They were also the first (and maybe the only ones as far as we know) to check the influence of the relative channels (α, p and n) on the evolution of a massive star. The inclusion of a resonance at 1.5 MeV in the NRCS [156] showed that the C ignition curve, i.e. the curve in the Log(T)-Log(ρ) that marks the locus where the nuclear energy generation rate ϵ_{C12C12} equates the neutrino energy losses ϵ_ν, shifts significantly downward in temperature with respect to the one obtained in the CF88 case, and hence that M_{up} is significantly reduced.

Currently a reliable determination of the ^{12}C+^{12}C NRCS is still missing; two opposite scenarios are currently under debate, one that foresees an NRCS higher than the classical CF88 (obtained with the Trojan Horse method, THM) and another one, less effective than the CF88 one, obtained in the Hindrance scenario. In addition, intermediate possibilities between these two extremes have also been proposed.

Since there is still no consensus about the real NRCS for this nuclear reaction, it is important to completely re-analyze the influence of both these NRCS (the THM and the HIN

one) on the evolution of a star. In the following, we will first discuss the role played by C burning on the evolution of a star as a function of the initial mass by adopting the CF88 NRCS. All models were computed with the same version of the FRANEC adopted by Chieffi et al. [157,158], but in this case we chose to use the Schwarzschild criterion to fix the border of all the convective zones. This will be our reference scenario. Then we will show how this scenario changes if the NRCS obtained in the Hindrance scenario (HIN) or the one obtained by means of the Trojan Horse Method (THM) are adopted.

Let us clearly stress that we are not considering in the present context uncertainties connected to, e.g., the input physics, like the equation of state, the opacity, the neutrinos energy losses, the screening, the weak interactions, the mass-loss rates or about the validity of the mixing length formalism to mimic the thermal instabilities that occur in a star. We are also focusing on single solar metallicity models.

A second thing worth being clearly stated is that this section is not intended at all to discuss the differences among models computed by different authors over many decades. Here we are only interested in understanding how some key evolutionary properties depend on the NRCS under exam, and hence the only models that will be discussed here will be those specifically computed for this paper plus the very limited number of recent papers in which different NRCS for the $^{12}C + {}^{12}C$ have been explored, i.e. Chieffi et al. [157,158], Monpribat et al. [159] and Dumont et al. [160].

In principle the role and features of the C burning are well known. We think, however, that it is worth summarizing a few key evolutionary properties of a star that are of interest for the C burning (and beyond). C burning is the third main nuclear burning and occurs after the H and He burning in all stars able to reach a temperature of the order of 800 MK. Two key parameters control the C burning: the first one is the mass fraction of ^{12}C left by the He burning because it is the fuel to be burnt (it enters directly in the reaction rate of the $^{12}C+{}^{12}C$ nuclear reaction) while the second one is the *mass* of the star. Similarly to what happens for the central H and He burning, also in this case there is a minimum threshold *mass* above which C burning may occur. The *mass* that controls the possible C ignition, however, is not the initial mass but the CO core mass that forms after the central He burning. By the way, the same holds in He burning where it is the He core mass that determines the evolutionary properties of the He burning. Hence one should discuss, in principle, the properties of the models in terms of the CO core mass; on the contrary, it is common to discuss them in terms of the initial mass. The reason is that, in principle, there is a strong direct correlation between the CO core mass and the initial mass so that it should be indifferent to use one or the other; unfortunately, a number of uncertainties including at the very minimum the mass size of the convective core both in H and He burning plus the sinking of the second dredge up, do not allow to define a unique, robust relation between the initial and the CO core mass. In the present case we will use indifferently the initial masses or the CO core mass because we are performing partial derivatives, i.e. the relation between initial mass and CO mass at the beginning of the He shell burning phase is the same in all cases explored here. In general, the increase of the temperature in the inner core of a star is due to the release of gravitational energy caused by its contraction. According to the Virial theorem, in case of an ideal gas 50% of the energy gained by the gravitational contraction leads to the increase of the internal energy (and hence of the temperature) while the other 50% is transmitted outward. Since the amount of gravitational energy released by a contracting CO core scales directly with its mass size, the more massive the CO core the higher will be the maximum temperature that may be reached and the faster will be its increase. However, the energy gain (and hence the temperature increase) induced by the gravitational contraction competes with the neutrino energy losses that on the contrary tend to cool down the central region of the core, so that the maximum value of the temperature as well as its location in mass depend on the competition between cooling and heating. Stars that form a CO core more massive than a threshold value (just after the end of the He burning) contract and evolve up to the core collapse independently on the rate of the $^{12}C+{}^{12}C$ or any nuclear reaction because in these stars the electron degeneracy does not play any significant role (hereinafter by degeneracy we will mean electron degeneracy). Vice versa stars whose initial CO core is smaller than the threshold value cannot contract freely because the degeneracy of the core tends to sustain the star without the requirement of additional contraction; in this case additional nuclear burning after the central He exhaustion may occur only if the CO core can grow and hence raise the maximum temperature up to the threshold value dictated by the adopted NRCS of the $^{12}C+{}^{12}C$. The typical value for this threshold CO mass is of the order of $1.3{:}1.4 M_\odot$.

Given the importance of the mass size and the temporal evolution of the CO core in determining the fate of a star, Fig. 13 shows the run of the maximum temperature versus the CO core mass for stellar models in the range 6 to $13 M_\odot$ for the reference scenario. Stellar models up to $8.2 M_\odot$ are not able to reach the threshold temperature for the C ignition: they increase their maximum temperature until the CO core can grow in mass (i.e. until the He burning shell may advance in mass) and then it start decreasing because the neutrino energy losses dominate the energy budget. The maximum mass that does not ignite C, M_{up}, is therefore confined between 8.2 and $8.3 M_\odot$. It is worth noting in Fig. 13 that the increase of the maximum temperature is associated to a significant increase of the CO core mass. Models with $M_{ini} \geq 10.3 M_\odot$ ignite Ne off center, burn it down to the center and evolve through all other nuclear burning up to the Nuclear Statistical

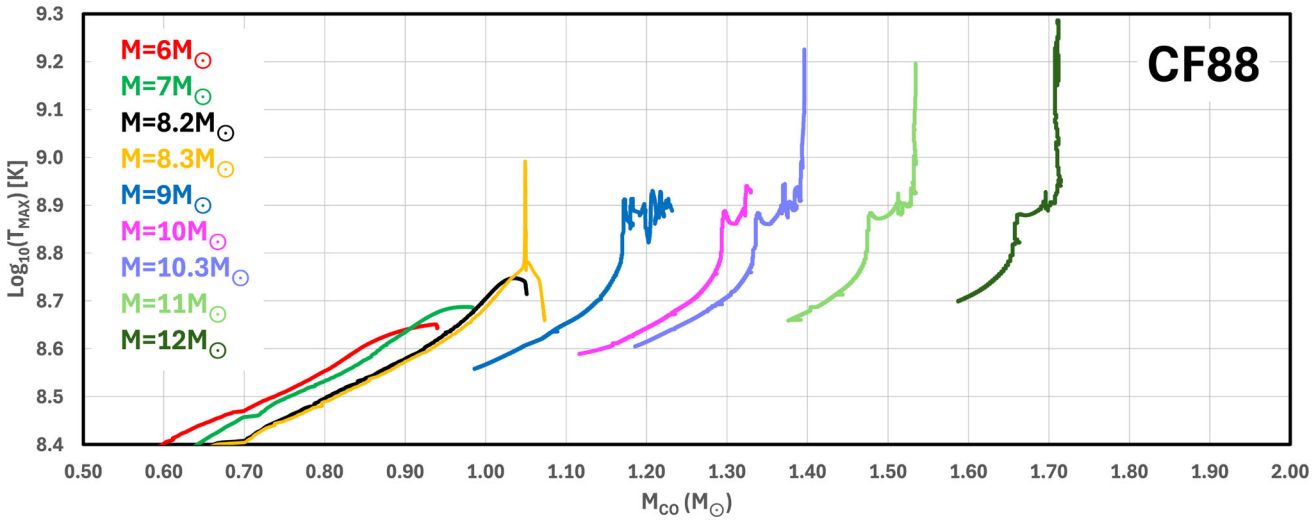

Fig. 13 Relation between the maximum temperature and the CO core mass (defined at the nuclear energy maximum of the He burning) for a series of masses computed with the CF88 nuclear cross section

Equilibrium and eventually collapse; the minimum mass that leads to the formation of a core collapse supernova, M_{MAS}, may be settled between 10 and 10.3$M_\odot$. The range of masses between M_{up} and M_{MAS}, i.e. between 8.2 and 10.3$M_\odot$ contains the transition region that separates stars that form a degenerate CO from those that evolve to the final collapse. This is a very complex mass interval (the so called range of the Super Asymptotic Giant Branch - SAGB - stars; see, e.g., [161–168] for a comprehensive analysis of this mass interval not much studied up to now) that includes both stars that ignite C off center and stars that ignite C centrally. All these stars eventually form a degenerate core without reaching directly the threshold temperature for the Ne ignition. The chemical composition within the degenerate core depends on the amount of C that has been burnt in C burning. The lowest fraction of SAGB stars (roughly up 8.8$M_\odot$) forms a degenerate core made of CONe (sometimes called hybrid stars), while the other forms a ONe core. The limiting mass between these two possible outcomes is M_{CONe}. While the masses below M_{CONe} will leave a compact remnant, the final fate of the stars that form a degenerate ONe core depends on the competition between the increase of the ONe core (due to the advancing of the H and He burning shells in the thermally pulsing phase) and the evaporation of the envelope mass due to the wind: a fraction of these stars may end as ONe white dwarf and a fraction explode as electron capture supernovae. Another critical mass worth being mentioned is the mass, M_X, that separates the stars that end their life with a degenerate core from those that eventually collapse. By the way, M_X is obviously confined between M_{CONe} and M_{MAS}. We cannot estimate the value of M_X from the present set of models because all runs where stopped either when the maximum temperature began to drop or at the beginning of the Ne burning. Note that the adoption of the CF88 NRCS settles the temperature of the C ignition in a degenerate environment to roughly 600 MK while the typical burning temperature once the degeneracy is removed is roughly 800 MK (see Fig. 13).

All these mass limits are of crucial importance because they fix the range of masses that share a similar behavior and their relative frequencies, i.e. the relative frequency among WD_{CO}, WD_{CONe} and WD_{ONe} as well as the expected frequency of the electron capture supernovae. The limiting mass M_{MAS} fixes the minimum mass that will explode as a core collapse supernova and simultaneously limits the range of masses that may form a WD_{One} or end their life as electron capture supernovae.

Stars more massive than M_{MAS} evolve up to the final collapse regardless of the actual efficiency of the various nuclear cross sections, including the $^{12}C+^{12}C$, but in spite of this, a change of this NRCS dramatically affects the advanced evolutionary phases of the massive stars and their final destiny. We did not compute new models in this mass range because a very detailed scenario was discussed by [157] and we will take advantage of that work. The physical structure of a massive star at the beginning of the core collapse, its compactness (which is somewhat connected to its capability of exploding), is mainly sculpted by the way in which the C burning shell advances in mass: qualitatively speaking, the more massive the C exhausted core, the higher its binding energy, the greater the energy needed to have a successful explosion.

The advancing of the C shell is controlled by the birth, growth and death of the various C convective shell. Now, the number, extension and duration of them change quite rapidly with the initial mass. Towards the lower end of the massive stars interval, stellar models form a C convective

core followed by 2–3 relatively small C convective shells; as the mass increases, central C burning becomes radiative (because of the combined effects of the lower amount of fuel left by the He burning and the tremendous direct dependence of the neutrino energy losses on the temperature and density) and the number of C convective shells reduces as well but they become more extended (in mass). As the initial mass increases further only one very extended C convective shell forms. Though the final compactness of a star may be presented in different ways, e.g. by means of the density profile or the mass-radius relation at the onset of the collapse, we think to be useful to adopt a compact way to measure the compactness of a star, a single parameter ξ [169], that is the ratio between the mass M and its corresponding radius R at the mass location M=2.5$M_\odot$, i.e. $\xi_{2.5} = 2.5\ M_\odot\ /\ R_{2.5}$ [1000 km].

Figure 8 in Chieffi et al [157] shows as blue dots how the ξ parameter depends on the initial mass. The trend is not monotonic and shows maxima and minima that are strongly correlated with the behavior of the C burning shell and that could identify islands of explodability (close to the minima) separated by regions in which stars simply collapse without ejecting any part of their final structure (around the maxima). Note that, given the rapid change of the ξ parameter with the initial mass, it is not possible to infer the properties and final fate of a full generation of massive stars (not just a single star) without computing the full evolution up to the beginning of the collapse of a quite refined grid of models.

Once we have briefly sketched the role that C burning has on the evolution of a star, let us now show how this complex scenario changes if one adopts a different NRCS for the $^{12}C+^{12}C$. We assume that the α and proton channels of this nuclear reaction are equally probable and do not change whichever NRCS is adopted. However, we note that the possible change of the branching ratio between α and proton channels may impact the evolution of the stars, both physical and chemical; see, e.g., Pignatari et al. [154]). In general, the uncertainties that affect $M_{\rm up}$, $M_{\rm CONe}$ and $M_{\rm MAS}$ may be divided in two categories. The first one concerns the relation between the initial mass and the pair M_{CO} plus the mass fraction $X_{^{12}C}$ left by the He burning: it includes the initial metallicity, the size of the convective core, the extension of the second dredge up, the temporal evolution of the convective core in He burning, the NRCS of the $^{12}C(\alpha,\gamma)^{16}O$ and rotation. The second class of uncertainties includes all the phenomena that occur after the central He burning, including the NRCS of the $^{12}C+^{12}C$ nuclear reaction (plus again the treatment of the convective zones). In this section we concentrate on just the influence of the NRCS of the $^{12}C+^{12}C$ on M_{up}, M_{MAS} and the advanced evolutionary phases of a massive stars. Figure 14 shows the relative values of both the HIN and THM NRCSs with respect to the reference one (the CF88) as a function of the temperature.

Table 1 Both limiting masses M_{up} and M_{CONe} are computed with a resolution of 0.1$M_\odot$ while M_{MAS} is evaluated with a resolution of 0.2/0.3$M_\odot$

NRCS	M_{up}	M_{CONe}	M_{MAS}
CF88	8.3	8.8	10–10.3
THM	7.2	8.0	9.8–10
HIN	9.0	9.4	10–10.3

Let us discuss firstly how the reference scenario changes if the THM NRCS is adopted, i.e. a nuclear cross section significantly higher than the CF88 one.

Figure 15 shows the run of the maximum temperature versus the CO core mass when the THM NRCS is adopted. In this case the minimum mass that ignites and burn C is the 7.2$M_\odot$ so that M_{up} is now located between 7.1 and 7.2$M_\odot$. Note that the minimum CO mass required to burn C drops from roughly 1.03$M_\odot$ to $\sim$ 1 $M_\odot$. M_{CONe} now is of the order of 8$M_\odot$ while the minimum mass that ignites Ne (and may proceed up to the Nuclear Statistical Equilibrium) is in this case the 10$M_\odot$, so that M_{MAS} ranges now between 9.8 and 10$M_\odot$. The adoption of a higher nuclear cross section lowers both M_{up} and M_{MAS}: the first one by roughly 1$M_\odot$ while the second one by just 0.2$M_\odot$ or so. The range of masses that leave a CONe core increases by roughly 0.2:0.3$M_\odot$. With this NRCS C ignites under degenerate conditions at a temperature of the order of 500 MK while the not degenerate burning occurs slightly above 700 MK.

Figure 16 shows the run of the maximum temperature versus the CO core mass when the HIN NRCS is adopted. In this case the minimum mass that ignites and burn C is the 9$M_\odot$ so that M_{up} is now located between 8.9 and 9$M_\odot$. The minimum CO mass required to burn C raises above 1.1$M_\odot$. The maximum mass that forms a degenerate core of CONe is now of the order of 9.4$M_\odot$. The minimum mass that ignites Ne (and may proceed up to the Nuclear Statistical Equilibrium) is in this case the 10.3$M_\odot$, so that M_{MAS} ranges now between 10 and 10.3$M_\odot$. With respect to the standard case, this nuclear cross section lifts M_{up} by roughly 1$M_\odot$ and M_{MAS} by 0.2$M_\odot$ or even less. C now ignites under degenerate condition at a temperature of the order of 700 MK while the main burning occurs slightly above 850 MK.

Table 1 collects all the mass limits obtained for the three different cases. Let us warn the reader once again that here we are interested only in the partial derivatives with respect to the $^{12}C+^{12}C$ NRCS because the absolute values change from one author to the other primarily because of different relations $M_{ini} - M_{CO}$ and/or different mass fraction of ^{12}C left by the He burning. Table 1 tells us first of all that the full interval (ΔM_{SAGB}) M_{up}-M_{MAS} scales directly with the efficiency of the $^{12}C+^{12}C$ NRCS. The higher the NRCS the wider is the mass range of the SAGB. The reason is that,

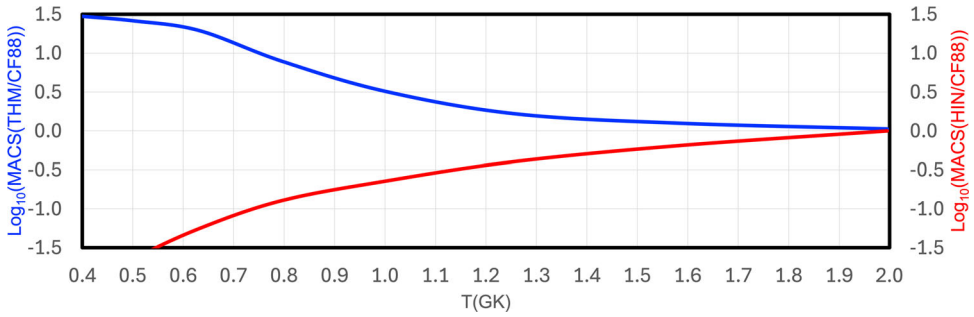

Fig. 14 Trend of the ratio between the THM nuclear cross section and the CF88 one as a function of the temperature (blue line). The same plot but for the HIN/CF88 ratio is shown as a red line

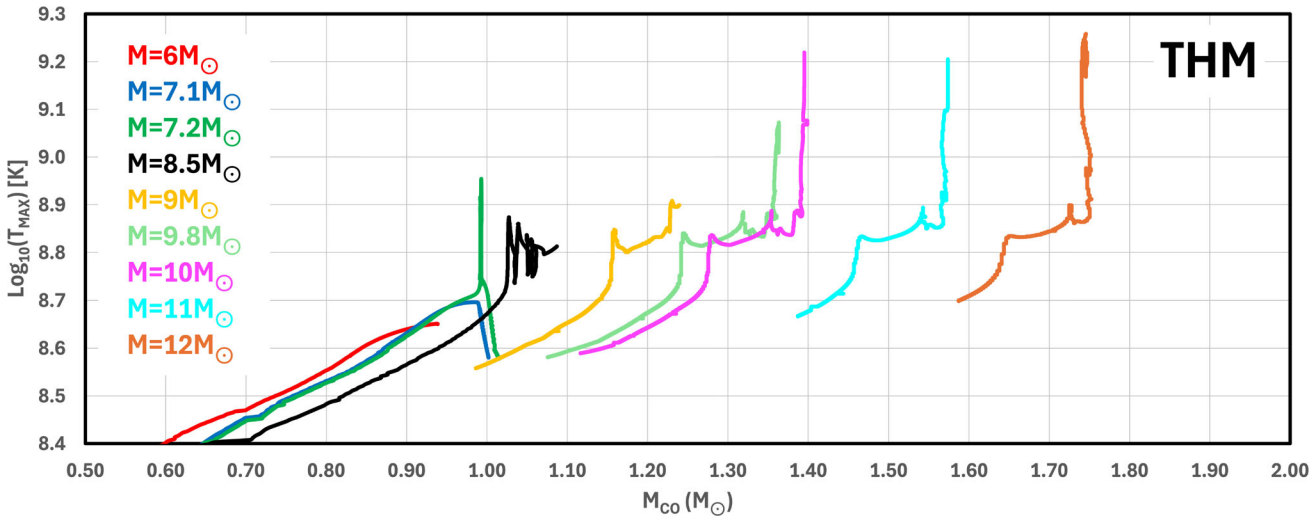

Fig. 15 Relation between the maximum temperature and the CO core mass (defined at the nuclear energy maximum of the He burning) for a series of masses computed with the THM nuclear cross section

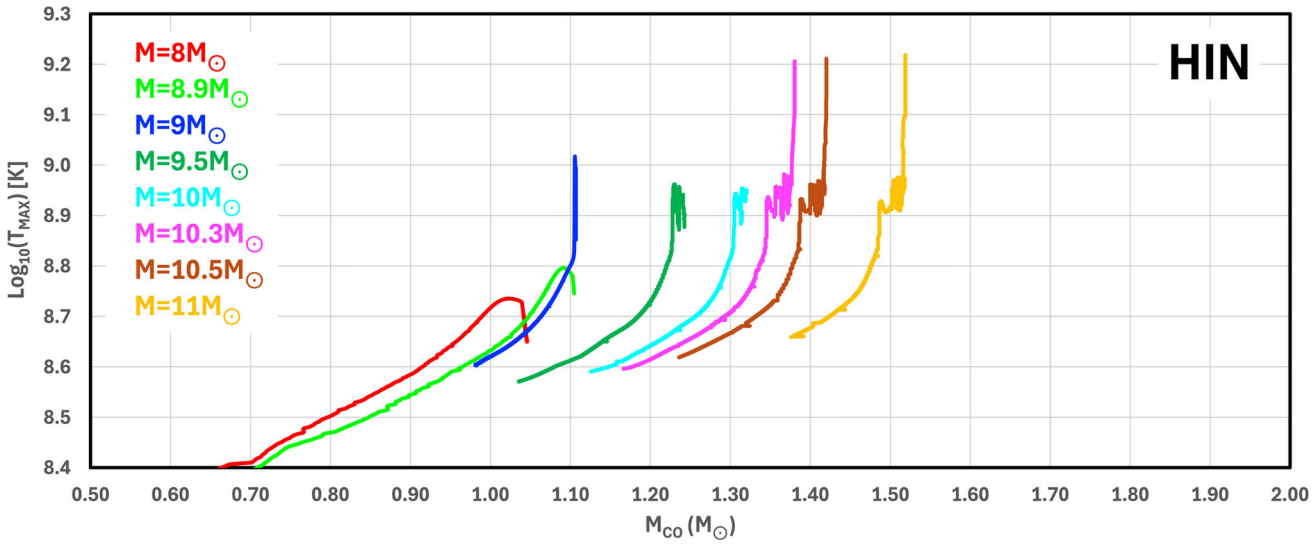

Fig. 16 Relation between the maximum temperature and the CO core mass (defined at the nuclear energy maximum of the He burning) for a series of masses computed with the HIN nuclear cross section

while M_{up} varies significantly with the NRCS, M_{MAS} does not. The reason why M_{MAS} depends much less than M_{up} on the NRCS may be easily understood by reminding that this limit is mainly dictated by the mass size of the CO core at the end of the central He burning that is obviously independent of the $^{12}C+^{12}C$ NRCS. So, while at one extreme we have a mass range of SAGB stars slightly less than $3M_\odot$ (THM case), at the other side (HIN case) this range drops to a mass interval slightly larger than $1M_\odot$. According to this results also all the other mass intervals shrink as the NRCS reduces. The range of masses that forms a CONe core drops from roughly $0.8M_\odot$ in the THM to roughly $0.4M_\odot$ in the HIN case. The mass range of the stars that form an ONe degenerate core drops from $2M_\odot$ to less than $1M_\odot$.

The real differences among the three scenarios may be appreciated once we consider the initial mass function (IMF). Let us consider a generation of stars in the interval 7 to $25M_\odot$. The lower limit of integration has been set to $7M_\odot$ because it is moderately smaller than the smallest of the three M_{up} and the upper limit has been chosen at $25M_\odot$ because there are reasons to think that stars more massive than this value will either explode as Type Ibc or even implode [170]. Note, however, that the ratio N_{SAGB}/N_{TOT} is only marginally affected by the two limits of integration (where N_{TOT} is the total number of stars between 7 and $25M_\odot$). Assuming a classical Salpeter IMF with a slope x=−1.35, the ratio N_{SAGB}/N_{MAS} amounts to 0.50 (CF88), 0.75 (THM) and 0.30 (HIN): there is a quite important difference among the three cases; the THM NRCS predicts more than a factor of two more compact object with respect to the massive stars than the HIN NRCS. Also the fraction of stars that form a CONe core with respect to the total number of SAGB stars changes somewhat since, while both the CF88 and the THM give a ratio of the order of 0.3, in the HIN case this ratio drops to 0.2 or so. The impact of these different scenarios on the global evolution of the galaxy goes beyond the purposes of the present analysis.

The dependence of M_{up} and M_{MAS} on the adopted $^{12}C+^{12}C$ NRCS has also been studied in other articles. The first one [171] showed that the adoption of the THM reduces M_{up} by roughly $0.5M_\odot$, a value smaller than the one obtained in the present tests, but it must be considered that their grid has a resolution of $0.5M_\odot$. As far as M_{MAS} is concerned, similarly to us, they found a negligible dependence of this limit on the $^{12}C+^{12}C$ nuclear cross section. The reason for such a finding is discussed above. The second [160] determined the two mass limits for both the CF88 and the HIN NRCS using the GENEVA stellar evolution code: GENEC [172]. Their results are in line with ours, M_{up} scaling directly with the efficiency of the NRCS while M_{MAS} changing very modestly, as expected (see above).

Let us now turn to the effect of a variation of the $^{12}C+^{12}C$ NRCS on the evolution of the massive stars. Also in this case we do not present any new model but we take advantage of a recent work [158] in which it is compared the evolution of two generations of stars in the mass range 12–$26M_\odot$, one evolved with the CF88 NRCS and a second one with the THM NRCS. The main effects of the THM NRCS is that of reducing the mass interval of stars that form a convective core. While in the CF88 case a convective core C develops in models up to $24M_\odot$, in the THM a C convective core develops up to a mass of $20M_\odot$. Also the number and extension of the C convective shells changes, the THM models forming, on average, a lower number of convective shell but more extended in mass. The final result is shown in Figure 9 of Chieffi et al. [158], where the final run of the compactness with the mass in the range 12 to $27M_\odot$ obtained with the THM NRCS is compared to the analogous run obtained by adopting the CF88 NRCS. The figure shows in both cases a quite large variation of the compactness with the mass, but also that the minima and maxima of the compactness occur at completely different masses. By means of just these computations it is not possible to infer the different impact of the two generation of massive stars computed with the two NRCS on the evolution of the galaxy, i.e. the different impact on the nucleosynthesis or on the expected number of core collapse supernovae. Note that the huge amount of computational time required to provide the scenario presented by Chieffi et al. [158] did not allow the use of the very extended network necessary to follow the nucleosynthesis properly.

The influence of the HIN NRCS on the evolution of massive stars has been studied by Gasquez et al. [77] (see above) and more recently by Monpribat et al. [159] and Dumont et al. [160], using the GENEC code. These papers present models computed with both the CF88 and the HIN NRCS. Their computations extend up to the Ne ignition or until the carbon flash for the less massive stars and their analysis focuses on the central C burning phase, which means that they cannot be used to determine the final structure of the models at the beginning of the collapse, neither in the CF88 nor in the HIN cases. However, their finding about the effect of the HIN NRCS on the central C burning is in line with the finding by Chieffi et al. [158], i.e. that the maximum mass that forms a convective core in C burning scales inversely with the efficiency of the nuclear cross section.

Finally, it is worth briefly reminding a phenomenon that affects a significant number of stars with an initial mass lower than $25M_\odot$ or so. In the final stages of their evolution these stars may, in fact, experience the merging of the carbon rich layers into the convective oxygen burning shell. This phenomenon, known as a "C-O shell merger", driven by vigorous turbulent motions, mixes the products of the C and O burning leading to a redistribution of many nuclear species over a wide mass interval. Such a phenomenon would lower the yields of the products of the C burning, because they would be spread down to regions where the passage of the shock wave will destroy them, and raise those of elements produced by

the O burning, because these elements will be spread out in regions where they would be preserved by the passage of the shock wave [173–178]. Moreover, this phenomenon would expose C-rich material to the high temperatures characteristic of the O burning. The implications of such an event that occurs few hours before the core-collapse, are significant. The newly formed mixed region contains distinctive nucleosynthesis products (e.g., odd-Z elements, p-nuclei, weak s-process components), which can survive the supernova shock wave and be ejected into the surrounding interstellar medium [173,178–180]. Additionally, the turbulent mixing generates a steep density and pressure gradient at the interface between the Si and O layers, potentially aiding the successful explosion of the star [181,182].

Ref. [178] suggested that the likelihood of a C-O shell merger is, at least partially, influenced by the carbon burning and hence on both the abundance of ^{12}C left by the burning He core and the ^{12}C +^{12}C NRCS. The lower the efficiency of the C burning shell, the lower the entropy barrier at the interface between the O and C convective shells. As a result, a changing in the ^{12}C+^{12}C NRCS could significantly affect the occurrence of C-O shell mergers and therefore the distinctive nucleosynthesis associated to such an event. However, a quantitative estimate of the effects such a changing on the chemical composition of the ejecta is extremely challenging because it would require the computation of an extensive grid of massive star models with a very detailed nuclear network able to follow in detail both the nuclear energy generation and the nucleosynthesis.

8 Conclusion

In the early studies of carbon fusion, the experiments were driven by the idea of discovering molecular states, cluster quantum configurations between two ^{12}C nuclei. An additional important driving factor in the experimental effort is the understanding of the pivotal role this nuclear reaction cross section has on the evolution of a wide range of stars. In terms of the quantum mechanics of the fusion mechanism the detailed understanding of the features of hindrance if any and the nature of the low energy resonances is of enormous importance and needs to be investigated [28].

However, it should be noted that, in particular in high density environments defining the ignition conditions for type Ia thermonuclear supernovae [19,183] and superbursts in the atmosphere of accreting neutron stars [27], the rate is expected to be substantially enhanced by electron screening and a certain extent will be of pycnonuclear nature, where the details of nuclear structure effects will be of lesser importance [9,28].

This paper provides an overview of the scientific developments in and the future of sub-barrier ^{12}C+^{12}C fusion studies. It is of particular interest for the understanding of the emergence quantum features near the threshold ranging from the formation of nuclear clusters or dynamic resonance structures as well as the possibility of hindrance due to the incompressibility of nuclear matter. While the experimental effort in is still inconclusive on the emergence of such features, theoretical predictions have so far focused on single aspects of such phenomena. A better understanding is of great importance for the development of a reliable reaction rate for the ^{12}C+^{12}C fusion process, which determines many crucial aspects of the evolution of stars in a wide mass interval, from the C ignition in electron degenerate conditions to the sculpting of the final mass-radius relation of the massive stars at the onset of the core collapse.

Funding RJD, WT, and MW utilized resources from the Notre Dame Center for Research Computing and were supported by the National Science Foundation through Grant No. PHY-2310059 (University of Notre Dame Nuclear Science Laboratory). ADT's work was supported by the United Kingdom Science and Technology Facilities Council (STFC) under Grant No. ST/Y000358/1. This work was supported in part by the National Science Foundation under Grant No. OISE-1927130 (IReNA). SC acknowledges support from the Marguerite Perey Chair of the University of Strasbourg Institute for Advanced Studies. TD is supported by the European Union, ChETEC-INFRA, Project No. 101008324.

Data Availability Statement response My manuscript has no associated data. [Author's comment: Data sharing not applicable to this article as no datasets were generated or analysed during the current study.]

Code Availability Statement response My manuscript has no associated code/software. [Author's comment: Code/Software sharing not applicable to this article as no code/software was generated or analysed during the current study.]

References

1. C.L. Jiang, B.B. Back, K.E. Rehm, K. Hagino, G. Montagnoli, A.M. Stefanini, Heavy-ion fusion reactions at extreme sub-barrier energies. Eur. Phys. J. A **57**(7), 235 (2021). https://doi.org/10.1140/epja/s10050-021-00536-2
2. C.L. Jiang, K.E. Rehm, B.B. Back, R.V.F. Janssens, Survey of heavy-ion fusion hindrance for lighter systems. Phys. Rev. C **79**(4), 044601 (2009). https://doi.org/10.1103/PhysRevC.79.044601

3. A. Tumino, C. Spitaleri, M. La Cognata, S. Cherubini, G.L. Guardo, M. Gulino, S. Hayakawa, I. Indelicato, L. Lamia, H. Petrascu, R.G. Pizzone, S.M.R. Puglia, G.G. Rapisarda, S. Romano, M.L. Sergi, R. Spartá, L. Trache, An increase in the ^{12}C + ^{12}C fusion rate from resonances at astrophysical energies. Nature **557**(7707), 687–690 (2018). https://doi.org/10.1038/s41586-018-0149-4
4. Ş Mişicu, H. Esbensen, Hindrance of Heavy-Ion Fusion due to Nuclear Incompressibility. Phys. Rev. Lett. **96**(11), 112701 (2006). https://doi.org/10.1103/PhysRevLett.96.112701
5. W.P. Tan, A. Boeltzig, C. Dulal, R.J. de Boer, B. Frentz, S. Henderson, K.B. Howard, R. Kelmar, J.J. Kolata, J. Long, K.T. Macon, S. Moylan, G.F. Peaslee, M. Renaud, C. Seymour, G. Seymour, B. Van de Kolk, M. Wiescher, E.F. Aguilera, P. Amador-Valenzuela, D. Lizcano, E. Martinez-Quiroz, New Measurement of ^{12}C + ^{12}C Fusion Reaction at Astrophysical Energies. Phys. Rev. Lett. **124**(19), 192702 (2020). https://doi.org/10.1103/PhysRevLett.124.192702
6. W.P. Tan, A. Gula, K. Lee, A. Majumdar, S. Moylan, O. Olivas-Gomez, S.M. Wiescher, E.F. Aguilera, D. Lizcano, E. Martinez-Quiroz, J.C. Morales-Rivera, Coincident measurement of the ^{12}C+^{12}C fusion cross section via the differential thick-target technique. Phys. Rev. C **110**(3), 035808 (2024). https://doi.org/10.1103/PhysRevC.110.035808
7. G. Fruet, S. Courtin, M. Heine, D.G. Jenkins, P. Adsley, A. Brown, R. Canavan, W.N. Catford, E. Charon, D. Curien, S.D. Negra, J. Duprat, F. Hammache, J. Lesrel, G. Lotay, A. Meyer, D. Montanari, L. Morris, M. Moukaddam, J. Nippert, Z.S. Podolyák, P.H. Regan, I. Ribaud, M. Richer, M. Rudigier, R. Shearman, N. de Séréville, C. Stodel, Advances in the Direct Study of Carbon Burning in Massive Stars. Phys. Rev. Lett. **124**(19), 192701 (2020). https://doi.org/10.1103/PhysRevLett.124.192701
8. A. Diaz-Torres, M. Wiescher, Characterizing the astrophysical *s* factor for ^{12}C +^{12} C fusion with wave-packet dynamics. Phys. Rev. C **97**(5), 055802 (2018). https://doi.org/10.1103/PhysRevC.97.055802
9. M. Beard, A.V. Afanasjev, L.C. Chamon, L.R. Gasques, M. Wiescher, D.G. Yakovlev, Astrophysical S factors for fusion reactions involving C, O, Ne, and Mg isotopes. At. Data Nucl. Data Tables **96**(5), 541–566 (2010). https://doi.org/10.1016/j.adt.2010.02.005
10. E.M. Burbidge, G.R. Burbidge, W.A. Fowler, F. Hoyle, Synthesis of the Elements in Stars. Rev. Modern Phys. **29**(4), 547–650 (1957). https://doi.org/10.1103/RevModPhys.29.547
11. H. Reeves, E.E. Salpeter, Nuclear Reactions in Stars. IV. Buildup from Carbon. Phys. Rev. **116**(6), 1505–1516 (1959). https://doi.org/10.1103/PhysRev.116.1505
12. W.D. Arnett, J.W. Truran, Carbon-Burning Nucleosynthesis at Constant Temperature. ApJ **157**, 339 (1969). https://doi.org/10.1086/150072
13. A.G.W. Cameron, Nuclear Reactions in Stars and Nucleogenesis. PASP **69**(408), 201 (1957). https://doi.org/10.1086/127051
14. R.J. de Boer, J. Görres, M. Wiescher, R.E. Azuma, A. Best, C.R. Brune, C.E. Fields, S. Jones, M. Pignatari, D. Sayre, K. Smith, F.X. Timmes, E. Uberseder, The ^{12}C(α, γ)^{16}O reaction and its implications for stellar helium burning. Rev. Modern Phys. **89**(3), 035007 (2017). https://doi.org/10.1103/RevModPhys.89.035007
15. M.E. Bennett, R. Hirschi, M. Pignatari, S. Diehl, C. Fryer, F. Herwig, A. Hungerford, K. Nomoto, G. Rockefeller, F.X. Timmes, M. Wiescher, The effect of ^{12}C + ^{12}C rate uncertainties on the evolution and nucleosynthesis of massive stars. MNRAS **420**(4), 3047–3070 (2012). https://doi.org/10.1111/j.1365-2966.2012.20193.x
16. M. Pignatari, R. Hirschi, M. Wiescher, R. Gallino, M. Bennett, M. Beard, C. Fryer, F. Herwig, G. Rockefeller, F.X. Timmes, The ^{12}C + ^{12}C Reaction and the Impact on Nucleosynthesis in Massive Stars. ApJ **762**(1), 31 (2013). https://doi.org/10.1088/0004-637X/762/1/31
17. F. Hoyle, W.A. Fowler, Nucleosynthesis in Supernovae. ApJ **132**, 565 (1960). https://doi.org/10.1086/146963
18. W.D. Arnett, A Possible Model of Supernovae: Detonation of ^{12}C. Ap&SS **5**(2), 180–212 (1969). https://doi.org/10.1007/BF00650291
19. E. Bravo, L. Piersanti, I. Domínguez, O. Straniero, J. Isern, J.A. Escartin, Type Ia supernovae and the ^{12}C + ^{12}C reaction rate. A&A **535**, A114 (2011). https://doi.org/10.1051/0004-6361/201117814
20. C.N. Augustine, D.E. Willcox, J. Brooks, D.M. Townsley, A.C. Calder, SN Ia Explosions from Hybrid Carbon-Oxygen-Neon White Dwarf Progenitors that Have Mixed during Cooling. ApJ **887**(2), 188 (2019). https://doi.org/10.3847/1538-4357/ab511a
21. D.G. Yakovlev, D.A. Shalybkov, Effect of plasma screening on thermonuclear reaction rates. Adv. Space Res. **8**(2), 707–710 (1988). https://doi.org/10.1016/0273-1177(88)90481-4. (**ISSN 0273-1177**)
22. A. Cumming, L. Bildsten, Carbon Flashes in the Heavy-Element Ocean on Accreting Neutron Stars. ApJ **559**(2), L127–L130 (2001). https://doi.org/10.1086/323937
23. T.E. Strohmayer, E.F. Brown, A Remarkable 3 Hour Thermonuclear Burst from 4U 1820–30. ApJ **566**(2), 1045–1059 (2002). https://doi.org/10.1086/338337
24. H. Schatz, L. Bildsten, A. Cumming, Photodisintegration-triggered Nuclear Energy Release in Superbursts. ApJ **583**(2), L87–L90 (2003). https://doi.org/10.1086/368107
25. A. Cumming, J. Macbeth, J.J.M. in 't Zand, D. Page, Long Type I X-Ray Bursts and Neutron Star Interior Physics. ApJ **646**(1), 429–451 (2006). https://doi.org/10.1086/504698
26. L. Keek, A. Heger, J.J.M. in't Zand, Superburst Models for Neutron Stars with Hydrogen- and Helium-rich Atmospheres. ApJ **752**(2), 150 (2012). https://doi.org/10.1088/0004-637X/752/2/150
27. R.L. Cooper, A.W. Steiner, E.F. Brown, Possible Resonances in the ^{12}C + ^{12}C Fusion Rate and Superburst Ignition. ApJ **702**(1), 660–671 (2009). https://doi.org/10.1088/0004-637X/702/1/660
28. M. Wiescher, C.A. Bertulani, C.R. Brune, R.J. de Boer, A. Diaz-Torres, L.R. Gasques, K. Langanke, P. Navrátil, W. Nazarewicz, J. Okolowicz, D.R. Phillips, M. Płszajczak, S. Quaglioni, A. Tumino, Quantum physics of stars. Rev. Modern Phys. **97**(1), 707 (2025). (**ISSN 1539-0756**)
29. D.G. Yakovlev, L.R. Gasques, A.V. Afanasjev, M. Beard, M. Wiescher, Fusion reactions in multicomponent dense matter. Phys. Rev. C. - Nucl. Phys. **74**(3), (2006). https://doi.org/10.1103/PhysRevC.74.035803. (**ISSN 0556-2813**)
30. E.J. Konopinski, C. Marvin, E. Teller, Ignition of the atmosphere with nuclear bombs. Technical Report LA-602, Los Alamos National Laboratory, (April 1946). URL http://www.gammaexplorer.com/lanlreports/lanl1_a/lib-www/la-pubs/00329010.html
31. L.D. Wyly, A. Zucker, Activities in Light Nuclei from Nitrogen Ion Bombardment. Phys. Rev. **89**(2), 524–525 (1953). https://doi.org/10.1103/PhysRev.89.524
32. H.L. Reynolds, D.W. Scott, A. Zucker, Nuclear Reactions with Energetic Nitrogen Ions. Proceedings of the National Academy of Science **39**(9), 975–985 (1953). https://doi.org/10.1073/pnas.39.9.975
33. H.L. Reynolds, D.W. Scott, A. Zucker, Nuclear Reactions Produced by Nitrogen on Boron and Oxygen. Phys. Rev. **102**(1), 237–241 (1956). https://doi.org/10.1103/PhysRev.102.237
34. E. Almqvist, D.A. Bromley, J.A. Kuehner, Resonances in C^{12} on Carbon Reactions. Phys. Rev. Lett. **4**(10), 515–517 (1960). https://doi.org/10.1103/PhysRevLett.4.515

35. D.A. Bromley, J.A. Kuehner, E. Almqvist, Resonant Elastic Scattering of C^{12} by Carbon. Phys. Rev. Lett. **4**(7), 365–367 (1960). https://doi.org/10.1103/PhysRevLett.4.365
36. E. Almqvist, J.A. Kuehner, D. McPherson, E.W. Vogt, Effects of Sample Size and Statistical Weights on Fluctuations in the $C^{12}(C^{12}, \alpha)Ne^{20}$ Reactions. Phys. Rev. **136**(1B), 84–98 (1964). https://doi.org/10.1103/PhysRev.136.B84
37. D. Shapira, R.G. Stokstad, D.A. Bromley, Statistical analysis of the energy dependence of $^{12}C + ^{12}C$ cross sections. Phys. Rev. C **10**(3), 1063–1082 (1974). https://doi.org/10.1103/PhysRevC.10.1063
38. J.R. Patterson, H. Winkler, C.S. Zaidins, Experimental Investigation of the Stellar Nuclear Reaction $^{12}C + ^{12}C$ at Low Energies. ApJ **157**, 367 (1969). https://doi.org/10.1086/150073
39. K.A. Erb, R.R. Betts, D.L. Hanson, M.W. Sachs, R.L. White, P.P. Tung, D.A. Bromley, New Resonances in the Low-Energy ^{12}C-^{12}C Spectrum. Phys. Rev. Lett. **37**(11), 670–673 (1976). https://doi.org/10.1103/PhysRevLett.37.670
40. H.W. Becker, K.U. Kettner, C. Rolfs, H.P. Trautvetter, The $^{12}C + ^{12}C$ reaction at subcoulomb energies. II. Zeitschrift fur Physik A. Hadrons. Nuclei. **303**, 305–312 (1981). https://doi.org/10.1007/BF01421528
41. G.J. Michaud, E.W. Vogt, Phenomenological Analysis of the $^{12}C + ^{12}C$ Reaction. Phys. Rev. C **5**(2), 350–368 (1972). https://doi.org/10.1103/PhysRevC.5.350
42. G. Michaud, Experimental Evidence for Repulsive Cores in Heavy-Ion Reactions. Phys. Rev. C **8**(2), 525–533 (1973). https://doi.org/10.1103/PhysRevC.8.525
43. D.A. Bromley, J.A. Kuehner, E. Almqvist, Elastic Scattering of Identical Spin-Zero Nuclei. Phys. Rev. **123**(3), 878–893 (1961). https://doi.org/10.1103/PhysRev.123.878
44. B. Imanishi, Resonance energies and partial widths of quasimolecular states formed by the two carbon nuclei. Phys. Lett. B **27**(5), 267–270 (1968). https://doi.org/10.1016/0370-2693(68)90094-4
45. H.J. Fink, W. Scheid, W. Greiner, Nuclear molecular structure in ^{12}C-^{12}C scattering. Nucl. Phys. A **188**(2), 259–288 (1972). https://doi.org/10.1016/0375-9474(72)90059-0
46. J.Y. Park, W. Greiner, W. Scheid, Quasimolecular states in the ^{12}C-^{12}C system. Phys. Rev. C **16**(6), 2276–2290 (1977). https://doi.org/10.1103/PhysRevC.16.2276
47. B. Dasmahapatra, B. Čujec, F. Lahlou, Fusion cross sections for $^{12}C + ^{12}C$, $^{12}C + ^{13}C$ and $^{13}C + ^{13}C$ at low energies. Nucl. Phys. A **384**(1), 257–272 (1982). https://doi.org/10.1016/0375-9474(82)90316-5
48. B. Dasmahapatra, B. Čujec, Measurement of cross sections for $^{12}C + ^{14}C$ reaction at subbarrier energies. Nucl. Phys. A **565**(3), 657–670 (1993). https://doi.org/10.1016/0375-9474(93)90051-X
49. S. Trentalange, S.C. Wu, J.L. Osborne, C.A. Barnes, Elastic scattering and fusion cross sections of $^{13}C + ^{13}C$. Nucl. Phys. A **483**(2), 406–428 (1988). https://doi.org/10.1016/0375-9474(88)90543-X
50. C. Beck, Y. Abe, N. Aissaoui, B. Djerroud, F. Haas, Role of the number of open channels in the dynamics of the dinucleus binary decay. Phys. Rev. C **49**, 2618–2629 (1994). https://doi.org/10.1103/PhysRevC.49.2618
51. G.R. Caughlan, W.A. Fowler, Thermonuclear Reaction Rates V. At. Data Nucl. Data Tables **40**, 283 (1988). https://doi.org/10.1016/0092-640X(88)90009-5
52. L.R. Gasques, A.V. Afanasjev, E.F. Aguilera, M. Beard, L.C. Chamon, P. Ring, M. Wiescher, D.G. Yakovlev, Nuclear fusion in dense matter: Reaction rate and carbon burning. Phys. Rev. C **72**(2), 025806 (2005). https://doi.org/10.1103/PhysRevC.72.025806
53. K.U. Kettner, H. Lorenz-Wirzba, C. Rolfs, H. Winkler, Study of the Fusion Reaction $^{12}C + ^{12}C$ below the Coulomb Barrier. Phys. Rev. Lett. **38**(7), 337–340 (1977). https://doi.org/10.1103/PhysRevLett.38.337
54. K.U. Kettner, H. Lorenz-Wirzba, C. Rolfs, The $^{12}C + ^{12}C$ reaction at subcoulomb energies (I). Z. Phys. A: Hadrons Nucl. **298**(1), 65–75 (1980). https://doi.org/10.1007/BF01416030
55. M.D. High, B. Čujec, The $^{12}C + ^{12}C$ sub-coulomb fusion cross section. Nucl. Phys. A **282**(1), 181–188 (1977). https://doi.org/10.1016/0375-9474(77)90179-8
56. M.S. Hussein, Under-the-barrier absorption effects in low energy heavy ion fusion reactions. Phys. Lett. B **71**(2), 249–251 (1977). https://doi.org/10.1016/0370-2693(77)90206-4
57. T. Spillane, F. Raiola, C. Rolfs, D. Schürmann, F. Strieder, S. Zeng, H.W. Becker, C. Bordeanu, L. Gialanella, M. Romano, J. Schweitzer, $^{12}C + ^{12}C$ Fusion Reactions near the Gamow Energy. Phys. Rev. Lett. **98**(12), 122501 (2007). https://doi.org/10.1103/PhysRevLett.98.122501
58. J. Zickefoose, A. Di Leva, F. Strieder, L. Gialanella, G. Imbriani, N. De Cesare, C. Rolfs, J. Schweitzer, T. Spillane, O. Straniero, F. Terrasi, Measurement of the $^{12}C(^{12}C,p)^{23}Na$ cross section near the Gamow energy. Phys. Rev. C **97**(6), 065806 (2018). https://doi.org/10.1103/PhysRevC.97.065806
59. L. Morales-Gallegos, M. Aliotta, C.G. Bruno, R. Buompane, T. Davinson, M. De Cesare, A. Di Leva, A. D'Onofrio, J.G. Duarte, L.R. Gasques, L. Gialanella, G. Imbriani, G. Porzio, D. Rapagnani, M. Romoli, D. Schürmann, F. Terrasi, L.Y. Zhang, Reduction of deuterium content in carbon targets for $^{12}C + ^{12}C$ reaction studies of astrophysical interest. Eur. Phys. J. A **54**(8), 132 (2018). https://doi.org/10.1140/epja/i2018-12564-8
60. E.F. Aguilera, P. Rosales, E. Martinez-Quiroz, G. Murillo, M. Fernández, H. Berdejo, D. Lizcano, A. Gómez-Camacho, R. Policroniades, A. Varela, E. Moreno, E. Chávez, M.E. Ortíz, A. Huerta, T. Belyaeva, M. Wiescher, New γ-ray measurements for $^{12}C + ^{12}C$ sub-Coulomb fusion: Toward data unification. Phys. Rev. C **73**(6), 064601 (2006). https://doi.org/10.1103/PhysRevC.73.064601
61. L. Morales-Gallegos, M. Aliotta, L. Gialanella, A. Best, C.G. Bruno, R. Buompane, T. Davinson, M. De Cesare, A. Di Leva, A. D'Onofrio, J.G. Duarte, L.R. Gasques, G. Imbriani, G. Porzio, D. Rapagnani, M. Romoli, F. Terrasi, Direct measurements of the ^{12}C+^{12}C reactions cross-sections towards astrophysical energies. Eur. Phys. J. A **60**(1), 11 (2024). https://doi.org/10.1140/epja/s10050-024-01233-6
62. C.L. Jiang, K.E. Rehm, B.B. Back, R.V.F. Janssens, Expectations for C12 and O16 induced fusion cross sections at energies of astrophysical interest. Phys. Rev. C **75**(1), 015803 (2007). https://doi.org/10.1103/PhysRevC.75.015803
63. C.L. Jiang, K.E. Rehm, H. Esbensen, R.V. Janssens, B.B. Back, C.N. Davids, J.P. Greene, D.J. Henderson, C.J. Lister, R.C. Pardo, T. Pennington, D. Peterson, D. Seweryniak, B. Shumard, S. Sinha, X.D. Tang, I. Tanihata, S. Zhu, P. Collon, S. Kurtz, M. Paul, Hindrance of heavy-ion fusion at extreme sub-barrier energies in open-shell colliding systems. Phys. Rev. C **71**(4), 044613 (2005). https://doi.org/10.1103/PhysRevC.71.044613
64. B.B. Back, H. Esbensen, C.L. Jiang, K.E. Rehm, Recent developments in heavy-ion fusion reactions. Rev. Mod. Phys. **86**(1), 317–360 (2014). https://doi.org/10.1103/RevModPhys.86.317
65. C.L. Jiang, B.B. Back, K.E. Rehm, K. Hagino, G. Montagnoli, A.M. Stefanini, Heavy-ion fusion reactions at extreme sub-barrier energies. Eur. Phys. J. A **57**(7), 235 (2021). https://doi.org/10.1140/epja/s10050-021-00536-2
66. M. Dasgupta, D.J. Hinde, A. Diaz-Torres, B. Bouriquet, C.I. Low, G.J. Milburn, J.O. Newton, Beyond the Coherent Coupled Channels Description of Nuclear Fusion. Phys. Rev. Lett. **99**(19), 192701 (2007). https://doi.org/10.1103/PhysRevLett.99.192701
67. G. Montagnoli, A.M. Stefanini, Recent experimental results in sub- and near-barrier heavy-ion fusion reactions. Eur. Phys. J. A **53**(8), 169 (2017). https://doi.org/10.1140/epja/i2017-12350-2

68. K. Godbey, C. Simenel, A.S. Umar, Absence of hindrance in a microscopic $^{12}C + ^{12}C$ fusion study. Phys. Rev. C **100**(2), 024619 (2019). https://doi.org/10.1103/PhysRevC.100.024619
69. K. Hagino, N. Takigawa, Subbarrier Fusion Reactions and Many-Particle Quantum Tunneling. Progress Theoret. Phys. **128**(6), 1061–1106 (2012). https://doi.org/10.1143/PTP.128.1061
70. A.S. Umar, K. Godbey, C. Simenel, Cluster model of ^{12}C in the density functional theory framework. Phys. Rev. C **107**(6), 064605 (2023). https://doi.org/10.1103/PhysRevC.107.064605
71. T. Depastas, S.T. Sun, H. Zheng, A. Bonasera, α-cluster microscopic study of $^{12}C + ^{12}C$ fusion toward the zero energy limit. Phys. Rev. C **108**(3), 035806 (2023). https://doi.org/10.1103/PhysRevC.108.035806
72. B. Bucher, X. D. Tang, X. Fang, A. Heger, S. Almaraz-Calderon, A. Alongi, A.D. Ayangeakaa, M. Beard, A. Best, J. Browne, and others. First Direct Measurement of 12C(12C,n)23Mg at Stellar Energies. Phys. Rev. Lett., **114**(25), 251102, (2015). https://doi.org/10.1103/PhysRevLett.114.251102
73. M.G. Mazarakis, W.E. Stephens, Experimental Measurements of the $^{12}C + ^{12}C$ Nuclear Reactions at Low Energies. Phys. Rev. C **7**(4), 1280–1287 (1973). https://doi.org/10.1103/PhysRevC.7.1280
74. L.J. Satkowiak, P.A. DeYoung, J.J. Kolata, M.A. Xapsos, Gamma-ray studies of the $^{12}C+^{12}C$ system. Phys. Rev. C **26**, 2027 (1982). https://doi.org/10.1103/PhysRevC.26.2027
75. L. Barrón-Palos, E.F. Aguilera, J. Aspiazu, A. Huerta, E. Martínez-Quiroz, R. Monroy, E. Moreno, G. Murillo, M.E. Ortiz, R. Policroniades, A. Varela, E. Chávez, Absolute cross sections measurement for the 12C + 12C system at astrophysically relevant energies. Nucl. Phys. A **779**, 318–332 (2006). https://doi.org/10.1016/j.nuclphysa.2006.09.004. (**ISSN 0375-9474.**)
76. C.L. Jiang, D. Santiago-Gonzalez, S. Almaraz-Calderon, K.E. Rehm, B.B. Back, K. Auranen, M.L. Avila, A.D. Ayangeakaa, S. Bottoni, M.P. Carpenter, C. Dickerson, B. DiGiovine, J.P. Greene, C.R. Hoffman, R.V.F. Janssens, B.P. Kay, S.A. Kuvin, T. Lauritsen, R.C. Pardo, J. Sethi, D. Seweryniak, R. Talwar, C. Ugalde, S. Zhu, D. Bourgin, S. Courtin, F. Haas, M. Heine, G. Fruet, D. Montanari, Reaction rate for carbon burning in massive stars. Phys. Rev. C **97**, 012801(R) (2018). https://doi.org/10.1103/PhysRevC.97.012801
77. L.R. Gasques, E.F. Brown, A. Chieffi, C.L. Jiang, M. Limongi, C. Rolfs, M. Wiescher, D.G. Yakovlev, Implications of low-energy fusion hindrance on stellar burning and nucleosynthesis. Phys. Rev. C **76**(3), 035802 (2007). https://doi.org/10.1103/PhysRevC.76.035802
78. A. Chieffi, L. Roberti, M. Limongi, M. La Cognata, L. Lamia, S. Palmerini, R.G. Pizzone, R. Spartà, A. Tumino, Impact of the New Measurement of the $^{12}C + ^{12}C$ Fusion Cross Section on the Final Compactness of Massive Stars. ApJ **916**(2), 79 (2021). https://doi.org/10.3847/1538-4357/ac06ca
79. E. Monpribat, S. Martinet, S. Courtin, M. Heine, S. Ekström, D.G. Jenkins, A. Choplin, P. Adsley, D. Curien, M. Moukaddam, J. Nippert, S. Tsiatsiou, G. Meynet, A new $^{12}C + ^{12}C$ nuclear reaction rate: Impact on stellar evolution. A&A **660**, A47 (2022). https://doi.org/10.1051/0004-6361/202141858
80. L. Morales-Gallegos, M. Aliotta, A. Best, C.G. Bruno, R. Buompane, T. Davinson, M. De Cesare, A. Di Leva, A. D'Onofrio, J. Duarte, L. Gasques, L. Gialanella, G. Imbriani, G. Porzio, D. Rapagnani, M. Romoli, F. Terrasi, $^{12}C + ^{12}C$ reactions for Nuclear Astrophysics. in *European Physical Journal Web of Conferences, volume 279 of European Physical Journal Web of Conferences*, page 11005, (2023). https://doi.org/10.1051/epjconf/202327911005
81. M. Aliotta, R. Buompane, M. Couder, A. Couture, R.J. de Boer, A. Formicola, L. Gialanella, J. Glorius, G. Imbriani, M. Junker, C. Langer, A. Lennarz, Y.A. Litvinov, W.P. Liu, M. Lugaro, C. Matei, Z. Meisel, L. Piersanti, R. Reifarth, D. Robertson, A. Simon, O. Straniero, A. Tumino, M. Wiescher, Y. Xu, The status and future of direct nuclear reaction measurements for stellar burning. J. Phys. G: Nucl. Phys. **49**(1), 010501 (2022). https://doi.org/10.1088/1361-6471/ac2b0f
82. G. Baur, Breakup reactions as an indirect method to investigate low-energy charged-particle reactions relevant for nuclear astrophysics. Phys. Lett. B **178**(2–3), 135–138 (1986). https://doi.org/10.1016/0370-2693(86)91483-8
83. S. Typel, G. Baur, Theory of the Trojan-Horse method. Ann. Phys. **305**(2), 228–265 (2003). https://doi.org/10.1016/S0003-4916(03)00060-5
84. C. Spitaleri, A.M. Mukhamedzhanov, L.D. Blokhintsev, M. La Cognata, R.G. Pizzone, A. Tumino, The Trojan Horse Method in nuclear astrophysics. Phys. At. Nucl. **74**(12), 1725–1739 (2011). https://doi.org/10.1134/S1063778811110184
85. C.A. Bertulani, M.S. Hussein, S. Typel, Assessing the foundation of the Trojan Horse Method. Phys. Lett. B **776**, 217–221 (2018). https://doi.org/10.1016/j.physletb.2017.11.050
86. R.E. Tribble, C.A. Bertulani, M. La Cognata, A.M. Mukhamedzhanov, C. Spitaleri, Indirect techniques in nuclear astrophysics: a review. Rep. Prog. Phys. **77**(10), 106901 (2014). https://doi.org/10.1088/0034-4885/77/10/106901
87. A. Tumino, C.A. Bertulani, M. La Cognata, L. Lamia, R.G. Pizzone, S. Romano, S. Typel, The Trojan Horse Method: A Nuclear Physics Tool for Astrophysics. Annu. Rev. Nucl. Part. Sci. **71**, 345–376 (2021). https://doi.org/10.1146/annurev-nucl-102419-033642
88. A. Tumino, C.A. Bertulani, S. Cherubini, G.F. D'Agata, A. Di Pietro, P. Figuera, G.L. Guardo, M. Gulino, S. Hayakawa, M. La Cognata, M. La Commara, L. Lamia, D. Lattuada, M. Mazzocco, A.M. Moro, J. Mrazek, A.A. Oliva, S. Palmerini, R.G. Pizzone, G.G. Rapisarda, S. Romano, M.L. Sergi, R. Spartà, S. Typel, H. Yamaguchi, Indirect methods with transfer reactions: The trojan horse method and the asymptotic normalization coefficient. Prog. Part. Nucl. Phys. **143**, 104164 (2025). https://doi.org/10.1016/j.ppnp.2025.104164. (**ISSN 0146-6410**)
89. Y.J. Li, X. Fang, B. Bucher, K.A. Li, L.H. Ru, X.D. Tang, Modified astrophysical S-factor of $^{12}C+^{12}C$ fusion reaction at sub-barrier energies. Chin. Phys. C **44**, 115001 (2020). https://doi.org/10.1088/1674-1137/abae56
90. K.A. Erb, R.R. Betts, S.K. Korotky, M.M. Hindi, P.P. Tung, M.W. Sachs, S.J. Willett, D.A. Bromley, Resonant and average behavior of the $^{12}C+^{12}C$ total reaction cross section: $5.6 \geq E$c.m. ≥ 10.0 Mev. Phys. Rev. C **22**, 507–514 (1980). https://doi.org/10.1103/PhysRevC.22.507
91. N.T. Zhang, X.Y. Wang, D. Tudor, B. Bucher, I. Burducea, H. Chen, Z.J. Chen, D. Chesneanu, A.I. Chilug, L.R. Gasques, D.G. Ghita, C. Gomoiu, K. Hagino, S. Kubono, Y.J. Li, C.J. Lin, W.P. Lin, R. Margineanu, A. Pantelica, I.C. Stefanescu, M. Straticiuc, X.D. Tang, L. Trache, A.S. Umar, W.Y. Xin, S.W. Xu, Y. Xu, Constraining the $12C + ^{12}C$ astrophysical S-factors with the $^{12}C+^{13}C$ measurements at very low energies. Phys. Lett. B **801**, 135170 (2020). https://doi.org/10.1016/j.physletb.2019.135170
92. M.J.F. Healy, Minimising carbon contamination during ion beam analysis. Nucl. Instrum. Methods B **129**, 130–136 (1997). https://doi.org/10.1016/S0168-583X(97)00127-4
93. E.F. Aguilera, P. Rosales, E. Martinez-Quiroz, G. Murillo, M.C. Fernández, Carbon buildup monitoring using RBS: Correlation with secondary electrons. Nucl. Inst. Meth. Phys. B. **244**, 427–435 (2006). https://doi.org/10.1016/j.nimb.2005.10.019
94. E. Almqvist, D.A. Bromley, J.A. Kuehner, B. Whalen, Spins and Partial Widths of Quasimolecular Resonances in $C^{12}+C^{12}$ Interactions. Phys. Rev. **130**, 1140 (1963). https://doi.org/10.1103/physrev.130.1140

95. C.A. Barnes, S. Trentalange, S.-C. Wu, Heavy-Ion Reactions in Nuclear Astrophysics. in D. Allan Bromley, editor, *Treatise on Heavy-Ion Science: Volume 6: Astrophysics, Chemistry, and Condensed Matter, volume 6*, pages 1–60. Springer US, Boston, MA, (1985). ISBN 978-1-4615-8103-1. https://doi.org/10.1007/978-1-4615-8103-1_1
96. C.L. Jiang, K.E. Rehm, X. Fang, X.D. Tang, M. Alcorta, B.B. Back, B. Bucher, P. Collon, C.M. Deibel, B. DiGiovine, J.P. Greene, D.J. Henderson, R.V.F. Janssens, T. Lauritsen, C.J. Lister, S.T. Marley, R.C. Pardo, D. Seweryniak, C. Ugalde, S. Zhu, M. Paul, Measurements of fusion cross-sections in ^{12}C+^{12}C at low beam energies using a particle-γ coincidence technique. NIM A **682**, 12–15 (2012). https://doi.org/10.1016/j.nima.2012.03.051
97. M. Heine, S. Courtin, G. Fruet, D.G. Jenkins, L. Morris, D. Montanari, M. Rudigier, P. Adsley, D. Curien, S. Della Negra, J. Lesrel, C. Beck, L. Charles, P. Dené, F. Haas, F. Hammache, G. Heitz, M. Krauth, A. Meyer, Zs Podolyák, P.H. Regan, M. Richer, N. de Séréville, C. Stodel, The stella apparatus for particle-gamma coincidence fusion measurements with nanosecond timing. Nuclear Instruments and Methods in Physics Research, Section A: Accelerators, Spectrometers, Detectors and Associated Equipment, pages 1–7, September 2018. URL https://eprints.whiterose.ac.uk/137500/. 2018 Elsevier B.V. This is an author-produced version of the published paper. Uploaded in accordance with the publisher?s self-archiving policy
98. G. Fruet, S. Courtin, M. Heine, D.G. Jenkins, P. Adsley, A. Brown, R. Canavan, W.N. Catford, E. Charon, D. Curien, and others. Advances in the Direct Study of Carbon Burning in Massive Stars. Phys. Rev. Lett., **124**(19), 192701, (2020). https://doi.org/10.1103/PhysRevLett.124.192701
99. O.J. Roberts, A.M. Bruce, P.H. Regan, Z.S. Podolyák, C.M. Townsley, J.F. Smith, K.F. Mulholland, A. Smith, A $LaBr_3$: Ce fast-timing array for DESPEC at FAIR. NIM A **748**, 91–95 (2014). https://doi.org/10.1016/j.nima.2014.02.037
100. M. Rudigier and Zs. Podolyák and P.H. Regan and A.M. Bruce and S. Lalkovski and R.L. Canavan and E.R. Gamba and O. Roberts and I. Burrows and D.M. Cullen and L.M. Fraile and L. Gerhard and J. Gerl and M. Gorska and A. Grant and J. Jolie and V. Karayonchev and N. Kurz and W. Korten and I.H. Lazarus and C.R. Nita and V.F.E. Pucknell and J.-M. Régis j and H. Schaffner and J. Simpson and P. Singh and C.M. Townsley and J.F. Smith and J. Vesic. FATIMA — FAst TIMing Array for DESPEC at FAIR. NIM A, 969:163967, 2020. https://doi.org/10.1016/j.nima.2020.163967
101. J. Nippert, A. Bonhomme, S. Courtin, D. Curien, E. Gregor, M. Heine, E. Monpribat, T. Dumont, C. Stodel, Recent Results on Direct Measurement of the ^{12}C+^{12}C Fusion Cross section at Deep Sub-barrier Energies with STELLA. Acta Phys. Pol. B Proc. Suppl. **17**, 3-A33 (2024). https://doi.org/10.5506/APhysPolBSupp.17.3-A33
102. J.M. Blatt, L.C. Biederharn, The Angular Distribution of Scattering and Reaction Cross Sections. Rev. Mod. Phys. **24**, 258–272 (1952). https://doi.org/10.1103/RevModPhys.24.258
103. M. Heine, G. Fruet, S. Courtin, D.G. Jenkins, P. Adsley, A. Brown, R. Canavan, W.N. Catford, E. Charon, D. Curien, S.D. Negra, J. Duprat, F. Hammache, J. Lesrel, G. Lotay, A. Meyer, E. Monpribat, D. Montanari, L. Morris, M. Moukaddam, J. Nippert, Z.S. Podolyák, P.H. Regan, I. Ribaud, M. Richer, M. Rudigier, R. Shearman, N. de Séréville, C. Stodel, Direct Measurement of Carbon Fusion at Astrophysical Energies with Gamma-Particle Coincidences. EPJ Web. Conf. **260**, 01004 (2022). https://doi.org/10.1051/epjconf/202226001004
104. G.J. Feldman, R.D. Cousins, Unified approach to the classical statistical analysis of small signals. Phys. Rev. D **57**, 3873 (1998). https://doi.org/10.1103/PhysRevD.57.3873
105. M. Heine, S. Courtin, G. Fruet, D.G. Jenkins, D. Montanari, L. Morris, P.H. Regan, M. Rudigier, D. Symochko, Gamma Efficiency Simulations towards Coincidence Measurements for Fusion Cross Sections. J. Phys: Conf. Ser. **763**, 012005 (2016). https://doi.org/10.1088/1742-6596/763/1/012005
106. X. Fang, W.P. Tan, M. Beard, R.J. de Boer, G. Gilardy, H. Jung, Q. Liu, S. Lyons, D. Robertson, K. Setoodehnia, C. Seymour, E. Stech, B. Van de Kolk, M. Wiescher, R.T. de Souza, S. Hudan, V. Singh, X.D. Tang, E. Uberseder, Experimental measurement of ^{12}C+^{16}O fusion at stellar energies. Phys. Rev. C **96**, 045804 (2017). https://doi.org/10.1103/PhysRevC.96.045804
107. X. Fang, *Measurement and Extrapolation of Total Cross Sections of 12C + 16O Fusion at Stellar Energies* (University of Notre Dame, Thesis, 2016)
108. M. Notani, H. Esbensen, X. Fang, B. Bucher, P. Davies, C.L. Jiang, L. Lamm, C.J. Lin, C. Ma, E. Martin, K.E. Rehm, W.P. Tan, S. Thomas, X.D. Tang, E. Brown, Correlation between the 12C+12C, 12C+13C, and 13C+13C fusion cross sections. Phys. Rev. C **85**(1), 014607 (2012). https://doi.org/10.1103/PhysRevC.85.014607
109. M. Romoli, L. Morales-Gallegos, M. Aliotta, C.G. Bruno, R. Buompane, A. D'Onofrio, T. Davinson, M. De Cesare, A. Di Leva, P. Di Meo, J. Duarte, L. Gasques, L. Gialanella, G. Imbriani, G. Porzio, D. Rapagnani, A. Vanzanella, Development of a two-stage detection array for low-energy light charged particles in nuclear astrophysics applications. Eur. Phys. J. A **54**(8), 142 (2018). https://doi.org/10.1140/epja/i2018-12575-5
110. J. Zickefoose, J. Schweitzer, T. Spillane, F. Strieder, H.-W. Becker, C. Rolfs, A. Di Leva, M. De Cesare, N. De Cesare, F. Terrasi, L. Gialanella, D. Schürmann, Y. Guan, Gianluca Imbriani, and Benedicta Limata. Low energy beam induced background studies for a 12C(12C,p)23Na reaction cross section measurement. in *Proceedings of 11th Symposium on Nuclei in the Cosmos — PoS(NIC XI)*, page 019, Heidelberg, Germany., July 2011. Sissa Medialab. https://doi.org/10.22323/1.100.0019
111. R.A. Dayras, Z.E. Switkowski, S.E. Woosley, Neutron branching in the reaction ^{12}c+^{12}c. Nucl. Phys. A **279**, 70–84 (1977)
112. W.P. Tan, A. Boeltzig, C. Dulal, R.J. de Boer, B. Frentz, S. Henderson, K.B. Howard, R. Kelmar, J.J. Kolata, J. Long, K.T. Macon, New Measurement of ^{12}C+^{12}C Fusion Reaction at Astrophysical Energies. Phys. Rev. Lett. **124**(19), 192702 (2020). https://doi.org/10.1103/PhysRevLett.124.192702
113. R.M. Gesuè, G.F. Ciani, D. Piatti, A. Boeltzig, D. Rapagnani, M. Aliotta, C. Ananna, L. Barbieri, F. Barile, D. Bemmerer, A. Best, C. Broggini, C.G. Bruno, A. Caciolli, M. Campostrini, F. Casaburo, F. Cavanna, P. Colombetti, A. Compagnucci, P. Corvisiero, L. Csedreki, T. Davinson, G.M. De Gregorio, D. Dell'Aquila, R. Depalo, A. Di Leva, Z. Elekes, F. Ferraro, A. Formicola, ZS. Fülöp, G. Gervino, A. Guglielmetti, C. Gustavino, GY. Gyürky, G. Imbriani, M. Junker, M. Lugaro, P. Marigo, J. Marsh, E. Masha, R. Menegazzo, D. Mercogliano, V. Paticchio, R. Perrino, P. Prati, V. Rigato, D. Robb, L. Schiavulli, R. S. Sidhu, J. Skowronski, O. Straniero, T. Szücs, S. Zavatarelli, and LUNA Collaboration. First Direct Measurement of the 64.5 keV Resonance Strength in the ^{17}O (p ,γ)^{18}F Reaction. Phys. Rev. Lett., **133**(5), 052701, (2024). https://doi.org/10.1103/PhysRevLett.133.052701
114. J. Skowronski, A. Boeltzig, G.F. Ciani, L. Csedreki, D. Piatti, M. Aliotta, C. Ananna, F. Barile, D. Bemmerer, A. Best, C. Broggini, C.G. Bruno, A. Caciolli, M. Campostrini, F. Cavanna, P. Colombetti, A. Compagnucci, P. Corvisiero, T. Davinson, R. Depalo, A. Di Leva, Z. Elekes, F. Ferraro, A. Formicola, ZS. Fülöp, G. Gervino, R. M. Gesuè, A. Guglielmetti, C. Gustavino, GY. Gyürky, G. Imbriani, M. Junker, M. Lugaro, P. Marigo, E. Masha, R. Menegazzo, V. Paticchio, R. Perrino, P. Prati, D. Rapagnani, V. Rigato, L. Schiavulli, R.S. Sidhu, O. Straniero,

T. Szücs, S. Zavatarelli, LUNA Collaboration. Proton-Capture Rates on Carbon Isotopes and Their Impact on the Astrophysical $^{12}C/^{13}C$ Ratio. Phys. Rev. Lett., **131**(16), 162701, (2023). https://doi.org/10.1103/PhysRevLett.131.162701

115. G.F. Ciani, L. Csedreki, D. Rapagnani, M. Aliotta, J. Balibrea-Correa, F. Barile, D. Bemmerer, A. Best, A. Boeltzig, C. Broggini, C. G. Bruno, A. Caciolli, F. Cavanna, T. Chillery, P. Colombetti, P. Corvisiero, S. Cristallo, T. Davinson, R. Depalo, A. Di Leva, Z. Elekes, F. Ferraro, E. Fiore, A. Formicola, Zs. Fülöp, G. Gervino, A. Guglielmetti, C. Gustavino, Gy. Gyürky, G. Imbriani, M. Junker, M. Lugaro, P. Marigo, E. Masha, R. Menegazzo, V. Mossa, F. R. Pantaleo, V. Paticchio, R. Perrino, D. Piatti, P. Prati, L. Schiavulli, K. Stöckel, O. Straniero, T. Szücs, M.P. Takács, F. Terrasi, D. Vescovi, S. Zavatarelli, LUNA Collaboration. Direct Measurement of the C 13 (α ,n)O 16 Cross Section into the s -Process Gamow Peak. Phys. Rev. Lett., **127**(15), 152701, (2021). https://doi.org/10.1103/PhysRevLett.127.152701
116. V. Mossa, K. Stöckel, F. Cavanna, F. Ferraro, M. Aliotta, F. Barile, D. Bemmerer, A. Best, A. Boeltzig, C. Broggini, C.G. Bruno, A. Caciolli, T. Chillery, G.F. Ciani, P. Corvisiero, L. Csedreki, T. Davinson, R. Depalo, A. Di Leva, Z. Elekes, E.M. Fiore, A. Formicola, Z.S. Fülöp, G. Gervino, A. Guglielmetti, C. Gustavino, G. Gyürky, G. Imbriani, M. Junker, A. Kievsky, I. Kochanek, M. Lugaro, L.E. Marcucci, G. Mangano, P. Marigo, E. Masha, R. Menegazzo, F.R. Pantaleo, V. Paticchio, R. Perrino, D. Piatti, O. Pisanti, P. Prati, L. Schiavulli, O. Straniero, T. Szücs, M.P. Takács, D. Trezzi, M. Viviani, S. Zavatarelli, The baryon density of the Universe from an improved rate of deuterium burning. Nature **587**(7833), 210–213 (2020). https://doi.org/10.1038/s41586-020-2878-4
117. A. Boeltzig, A. Best, F.R. Pantaleo, G. Imbriani, M. Junker, M. Aliotta, J. Balibrea-Correa, D. Bemmerer, C. Broggini, C.G. Bruno, R. Buompane, A. Caciolli, F. Cavanna, T. Chillery, G.F. Ciani, P. Corvisiero, L. Csedreki, T. Davinson, R.J. de Boer, R. Depalo, A. Di Leva, Z. Elekes, F. Ferraro, E.M. Fiore, A. Formicola, Z.S. Fülöp, G. Gervino, A. Guglielmetti, C. Gustavino, G.Y. Gyürky, I. Kochanek, M. Lugaro, P. Marigo, R. Menegazzo, V. Mossa, F. Munnik, V. Paticchio, R. Perrino, D. Piatti, P. Prati, L. Schiavulli, K. Stöckel, O. Straniero, F. Strieder, T. Szücs, M.P. Takács, D. Trezzi, M. Wiescher, S. Zavatarelli, Direct measurements of low-energy resonance strengths of the $^{23}Na(p,\gamma)^{24}Mg$ reaction for astrophysics. Phys. Lett. B **795**, 122–128 (2019). https://doi.org/10.1016/j.physletb.2019.05.044
118. ...F. Ferraro, M.P. Takács, D. Piatti, F. Cavanna, R. Depalo, M. Aliotta, D. Bemmerer, A. Best, A. Boeltzig, C. Broggini, C.G. Bruno, A. Caciolli, T. Chillery, G.F. Ciani, P. Corvisiero, T. Davinson, G. D'Erasmo, A. Di Leva, Z. Elekes, E.M. Fiore, A. Formicola, Z.S. Fülöp, G. Gervino, A. Guglielmetti, C. Gustavino, G.Y. Gyürky, G. Imbriani, M. Junker, A. Karakas, I. Kochanek, M. Lugaro, P. Marigo, R. Menegazzo, V. Mossa, F.R. Pantaleo, V. Paticchio, R. Perrino, P. Prati, L. Schiavulli, K. Stöckel, O. Straniero, T. Szücs, D. Trezzi, S. Zavatarelli, LUNA Collaboration, Direct Capture Cross Section and the E_p=71 and 105 keV Resonances in the $^{22}Ne(p,\gamma)^{23}Na$ Reaction. Phys. Rev. Lett. **121**(17), 172701 (2018). https://doi.org/10.1103/PhysRevLett.121.172701
119. M. Junker, G. Imbriani, A. Best, A. Boeltzig, A. Compagnucci, A. Di Leva, F. Ferraro, D. Rapagnani, V. Rigato, The deep underground Bellotti Ion Beam Facility–status and perspectives. Front. Phys. **11**, 1291113 (2023). https://doi.org/10.3389/fphy.2023.1291113
120. A. Sen, G. Domínguez-Cañizares, N.C. Podaru, D.J.W. Mous, M. Junker, G. Imbriani, V. Rigato, A high intensity, high stability 3.5 MV Singletron™ accelerator. Nuclear Instruments Methods Phys. Res. B **450**, 390–395 (2019). https://doi.org/10.1016/j.nimb.2018.09.016
121. A. Boeltzig, A. Best, G. Imbriani, M. Junker, M. Aliotta, D. Bemmerer, C. Broggini, C.G. Bruno, R. Buompane, A. Caciolli, F. Cavanna, T. Chillery, G.F. Ciani, P. Corvisiero, L. Csedreki, T. Davinson, R.J. de Boer, R. Depalo, A. Di Leva, Z. Elekes, F. Ferraro, E.M. Fiore, A. Formicola, Z. Fülöp, G. Gervino, A. Guglielmetti, C. Gustavino, G. Gyürky, I. Kochanek, R. Menegazzo, V. Mossa, F.R. Pantaleo, V. Paticchio, R. Perrino, D. Piatti, P. Prati, L. Schiavulli, K. Stöckel, O. Straniero, F. Strieder, T. Szücs, M.P. Takács, D. Trezzi, M. Wiescher, S. Zavatarelli, Improved background suppression for radiative capture reactions at LUNA with HPGe and BGO detectors. J. Phys. G Nuclear Phys. **45**(2), 025203 (2018). https://doi.org/10.1088/1361-6471/aaa163
122. A. Caciolli, L. Agostino, D. Bemmerer, R. Bonetti, C. Broggini, F. Confortola, P. Corvisiero, H. Costantini, Z. Elekes, A. Formicola, Z.S. Fülöp, G. Gervino, A. Guglielmetti, C. Gustavino, G.Y. Gyürky, M. Imbriani, M. Junker, M. Laubenstein, A. Lemut, B. Limata, M. Marta, C. Mazzocchi, R. Menegazzo, P. Prati, V. Roca, C. Rolfs, C.R. Alvarez, E. Somorjai, O. Straniero, F. Strieder, F. Terrasi, H.P. Trautvetter, Ultra-sensitive in-beam γ -ray spectroscopy for nuclear astrophysics at LUNA. Eur. Phys. J. A **39**(2), 179–186 (2009). https://doi.org/10.1140/epja/i2008-10706-3
123. M. Laubenstein, I. Lawson, Low Background Radiation Detection Techniques and Mitigation of Radioactive Backgrounds. Front. Phys. **8**, 506 (2020). https://doi.org/10.3389/fphy.2020.577734
124. T. Kawabata, T. Adachi, M. Fujiwara, K. Hatanaka, Y. Ishiguro, M. Itoh, Y. Maeda, H. Matsubara, H. Miyasako, Y. Nozawa, T. Saito, S. Sakaguchi, Y. Sasamoto, Y. Shimizu, T. Takahashi, A. Tamii, S. Terashima, H. Tokieda, N. Tomida, T. Uesaka, M. Uchida, Y. Yasuda, N. Yokota, H.P. Yoshida, J. Zenihiro, Search for alpha inelastic condensed state in ^{24}Mg. Jour. Phys. Conf. Ser. **436**, 012009 (2013). https://doi.org/10.1088/1742-6596/436/1/012009
125. J.M. Munson, E.B. Norman, J.T. Burke, R.J. Casperson, L.W. Phair, E. McCleskey, M. McCleskey, D. Lee, R.O. Hughes, S. Ota, A. Czeszumska, P.A. Chodash, A.J. Saastamoinen, R.A.E. Austin, A.E. Spiridon, M. Dag, R. Chyzh, M.S. Basunia, J.J. Ressler, T.J. Ross, Decay branching ratios of excited ^{24}Mg. Phys. Rev. C **95**, 015805 (2017). https://doi.org/10.1103/PhysRevC.95.015805
126. P. Adsley, M. Heine, D.G. Jenkins, S. Courtin, R. Neveling, J. W. Brümmer, L.M. Donaldson, N.Y. Kheswa, K.C.W. Li, D.J. Marín-Lámbarri, and others. Extending the Hoyle-State Paradigm to 12C+12C Fusion. Phys. Rev. Lett., 129(10):102701, (2022). https://doi.org/10.1103/PhysRevLett.129.102701
127. Y. Chiba, M. Kimura, Cluster states and isoscalar monopole transitions of ^{24}Mg. Phys. Rev. C **91**, 061302(R) (2015). https://doi.org/10.1103/PhysRevC.91.061302
128. R. Abegg, C.A. Davis, ^{24}Mg states observed via $^{20}Ne(\alpha,\alpha_0)^{20}Ne$. Phys. Rev. C **43**, 2523–2540 (1991). https://doi.org/10.1103/PhysRevC.43.2523
129. C.A. Davis, Inelastic α scattering from ^{20}Ne. Phys. Rev. C **45**, 2693–2700 (1992). https://doi.org/10.1103/PhysRevC.45.2693
130. J.R. Vanhoy, E.G. Bilpuch, C.R. Westerfeldt, G.E. Mitchell, Proton resonances in ^{24}Mg from E_x=12.7 to 15.7 MeV. Phys. Rev. C **36**, 920–932 (1987). https://doi.org/10.1103/PhysRevC.36.920
131. R.E. Tribble, C.A. Bertulani, M. La Cognata, A.M. Mukhamedzhanov, C. Spitaleri, Indirect techniques in nuclear astrophysics: a review. Rept. Prog. Phys. **77**(10), 106901 (2014). https://doi.org/10.1088/0034-4885/77/10/106901
132. M. La Cognata, S. Palmerini, C. Spitaleri, I. Indelicato, A.M. Mukhamedzhanov, I. Lombardo, O. Trippella, Updated THM Astrophysical Factor of the $^{19}F(p,\alpha)^{16}O$ Reaction and Influence of New Direct Data at Astrophysical Energies. ApJ **805**(2), 128 (2015). https://doi.org/10.1088/0004-637X/805/2/128
133. O. Trippella, M. La Cognata, Concurrent Application of ANC and THM to assess the $^{13}C(\alpha,n)^{16}O$ Absolute Cross Section at Astrophysical Energies and Possible Consequences for Neutron

Production in Low-mass AGB Stars. Astrophys. J. **837**(1), 41 (2017). https://doi.org/10.3847/1538-4357/aa5eb5
134. M. La Cognata, C. Spitaleri, A. Mukhamedzhanov, A. Banu, S. Cherubini, A. Coc, V. Crucillà, V. Goldberg, M. Gulino, B. Irgaziev, G.G. Kiss, L. Lamia, J. Mrazek, R.G. Pizzone, S.M.R. Puglia, G.G. Rapisarda, S. Romano, M.L. Sergi, G. Tabacaru, L. Trache, R.E. Tribble, W. Trzaska, A. Tumino, A novel approach to measure the cross section of the ^{18}O(p, α)^{15}N resonant reaction in the 0–200 keV energy range. Astrophys. J. **708**(1), 796–811 (2009). https://doi.org/10.1088/0004-637x/708/1/796
135. M. La Cognata, S. Palmerini, P. Adsley, F. Hammache, A. Di Pietro, P. Figuera, F. Dell'Agli, R. Alba, S. Cherubini, G.L. Guardo, M. Gulino, L. Lamia, D. Lattuada, C. Maiolino, A. Oliva, R.G. Pizzone, P.M. Prajapati, G.G. Rapisarda, S. Romano, D. Santonocito, R. Spartá, M.L. Sergi, A. Tumino, P. Ventura, A New Reaction Rate of the ^{27}Al(p/α)^{24}Mg Reaction Based on Indirect Measurements at Astrophysical Energies and Implications for ^{27}Al Yields of Intermediate-mass Stars. Astrophys. J. **941**(1), 96 (2022). https://doi.org/10.3847/1538-4357/ac9c5e
136. A.M. Mukhamedzanov, Status of deep subbarrier ^{12}C + ^{12}C fusion and advancing the Trojan horse method. Eur. Phys. J. A **58**(4), 71 (2022). https://doi.org/10.1140/epja/s10050-022-00718-6
137. A.M. Mukhamedzhanov, A.S. Kadyrov, Theory of Surrogate Nuclear and Atomic Reactions with Three Charged Particles in the Final State Proceeding Through a Resonance in the Intermediate Subsystem. Few-Body Syst. **60**(2), 27 (2019). https://doi.org/10.1007/s00601-019-1489-9
138. A. Bonasera, J.B. Natowitz, Calculation of the ^{12}C + ^{12}C subbarrier fusion cross section in an imaginary-time-dependent mean field theory. Phys. Rev. C **102**(6), 061602 (2020). https://doi.org/10.1103/PhysRevC.102.061602
139. Y. Taniguchi, M. Kimura, Impact of the molecular resonances on the ^{12}C + ^{12}C fusion reaction rate. Phys. Lett. B **849**, 138434 (2024). https://doi.org/10.1016/j.physletb.2023.138434
140. N.T. Zhang, X.Y. Wang, D. Tudor, B. Bucher, I. Burducea, H. Chen, Z.J. Chen, D. Chesneanu, A.I. Chilug, L.R. Gasques et al., Constraining the 12c+ 12c astrophysical s-factors with the 12c+ 13c measurements at very low energies. Phys. Lett. B **801**, 135170 (2020)
141. K. Godbey, C. Simenel, A.S. Umar, Absence of hindrance in a microscopic ^{12}C + ^{12}C fusion study. Phys. Rev. C **100**, 024619 (2019). https://doi.org/10.1103/PhysRevC.100.024619
142. M. Assunção, P. Descouvemont, Role of the Hoyle state in ^{12}C + ^{12}C fusion. Phys. Lett. B **723**(4–5), 355–359 (2013). https://doi.org/10.1016/j.physletb.2013.05.030
143. L.R. Gasques, L.C. Chamon, G.P. Cessel, The role of inelastic couplings on the ^{12}C + ^{12}C fusion at sub-barrier energies. Eur. Phys. J. A **58**(6), 102 (2022). https://doi.org/10.1140/epja/s10050-022-00751-5
144. A. Diaz-Torres, M. Wiescher, Characterizing the astrophysical *S* factor for ^{12}C + ^{12}C fusion with wave-packet dynamics. Phys. Rev. C **97**(5), 055802 (2018). https://doi.org/10.1103/PhysRevC.97.055802
145. A. Diaz-Torres, Solving the Two-Center Nuclear Shell-Model Problem with Arbitrarily Oriented Deformed Potentials. Phys. Rev. Lett. **101**(12), 122501 (2008). https://doi.org/10.1103/PhysRevLett.101.122501
146. G. Close, P. Stevenson, A. Diaz-Torres, Quantum dynamical microscopic approach to stellar carbon burning. Phys. Lett. B **870**, 139881 (2025). https://doi.org/10.1016/j.physletb.2025.139881
147. C.L. Jiang, B.B. Back, H. Esbensen, R.V.F. Janssens, K.E. Rehm, R.J. Charity, Origin and Consequences of ^{12}C + ^{12}C Fusion Resonances at Deep Sub-barrier Energies. Phys. Rev. Lett. **110**(7), 072701 (2013). https://doi.org/10.1103/PhysRevLett.110.072701
148. A. Diaz-Torres, L.R. Gasques, N.V. Antonenko, Cluster effects on low-energy carbon burning. Phys. Lett. B **849**, 138476 (2024). https://doi.org/10.1016/j.physletb.2024.138476
149. C. Spitaleri, C.A. Bertulani, L. Fortunato, A. Vitturi, The electron screening puzzle and nuclear clustering. Phys. Lett. B **755**, 275–278 (2016). https://doi.org/10.1016/j.physletb.2016.02.019
150. M. Aliotta, K. Langanke, Screening Effects in Stars and in the Laboratory. Front. Phys. **10**, 942726 (2022). https://doi.org/10.3389/fphy.2022.942726
151. S.A. Becker, I. Iben Jr., The asympiotic giant branch evolution of intermediate-mass stars as a function of mass and composition. II. Through the first major thermal pulse and the consequences of convective dredge-up. ApJ **237**, 111–129 (1980). https://doi.org/10.1086/157850
152. M. Limongi, A. Chieffi, The Nucleosynthesis of ^{26}Al and ^{60}Fe in Solar Metallicity Stars Extending in Mass from 11 to 120 M_{solar}: The Hydrostatic and Explosive Contributions. ApJ **647**(1), 483–500 (2006). https://doi.org/10.1086/505164
153. M.E. Bennett, R. Hirschi, M. Pignatari, S. Diehl, C. Fryer, F. Herwig, A. Hungerford, K. Nomoto, G. Rockefeller, F.X. Timmes, M. Wiescher, The effect of ^{12}C +^{12}C rate uncertainties on the evolution and nucleosynthesis of massive stars. MNRAS **420**(4), 3047–3070 (2012). https://doi.org/10.1111/j.1365-2966.2012.20193.x
154. M. Pignatari, R. Hirschi, M. Wiescher, R. Gallino, M. Bennett, M. Beard, C. Fryer, F. Herwig, G. Rockefeller, F.X. Timmes, The ^{12}C + ^{12}C Reaction and the Impact on Nucleosynthesis in Massive Stars. ApJ **762**(1), 31 (2013). https://doi.org/10.1088/0004-637X/762/1/31
155. F. Terrasi, D. Rogalla, N. De Cesare, A. D'Onofrio, C. Lubritto, F. Marzaioli, I. Passariello, M. Rubino, C. Sabbarese, G. Casa, A. Palmieri, L. Gialanella, G. Imbriani, V. Roca, M. Romano, M. Sundquist, R. Loger, A new AMS facility in Caserta/Italy. Nucl. Inst. Methods Phys. Res. B **259**(1), 14–17 (2007). https://doi.org/10.1016/j.nimb.2007.01.139
156. O. Straniero, L. Piersanti, S. Cristallo. Do we really know M_{up} (i.e. the transition mass between Type Ia and core-collapse supernova progenitors)? in *Journal of Physics Conference Series, volume 665 of Journal of Physics Conference Series*, page 012008. IOP, (2016). https://doi.org/10.1088/1742-6596/665/1/012008
157. A. Chieffi, M. Limongi, The Presupernova Core Mass-Radius Relation of Massive Stars: Understanding Its Formation and Evolution. ApJ **890**(1), 43 (2020). https://doi.org/10.3847/1538-4357/ab6739
158. A. Chieffi, L. Roberti, M. Limongi, M. La Cognata, L. Lamia, S. Palmerini, R.G. Pizzone, R. Spartà, A. Tumino, Impact of the New Measurement of the ^{12}C + ^{12}C Fusion Cross Section on the Final Compactness of Massive Stars. ApJ **916**(2), 79 (2021). https://doi.org/10.3847/1538-4357/ac06ca
159. E. Monpribat, S. Martinet, S. Courtin, M. Heine, S. Ekström, D.G. Jenkins, A. Choplin, P. Adsley, D. Curien, M. Moukaddam, J. Nippert, S. Tsiatsiou, G. Meynet, A new ^{12}C + ^{12}C nuclear reaction rate: Impact on stellar evolution. A&A **660**, A47 (2022). https://doi.org/10.1051/0004-6361/202141858
160. T. Dumont, E. Monpribat, S. Courtin, A. Choplin, A. Bonhomme, S. Ekström, M. Heine, D. Curien, J. Nippert, G. Meynet, Massive star evolution with a new ^{12}C + ^{12}C nuclear reaction rate. The core carbon-burning phase. A&A **688**, A115 (2024). https://doi.org/10.1051/0004-6361/202348968
161. L. Siess, Evolution of massive AGB stars. I. Carbon burning phase. A&A **448**(2), 717–729 (2006). https://doi.org/10.1051/0004-6361:20053043
162. L. Siess, Evolution of massive AGB stars. II. model properties at non-solar metallicity and the fate of Super-AGB stars. A&A **476**(2), 893–909 (2007). https://doi.org/10.1051/0004-6361:20078132

163. L. Siess, Evolution of massive AGB stars. III. the thermally pulsing super-AGB phase. A&A **512**, A10 (2010). https://doi.org/10.1051/0004-6361/200913556
164. C.L. Doherty, L. Siess, J.C. Lattanzio, P. Gil-Pons, Super asymptotic giant branch stars. I - Evolution code comparison. MNRAS **401**(3), 1453–1464 (2010). https://doi.org/10.1111/j.1365-2966.2009.15772.x
165. C.L. Doherty, P. Gil-Pons, H.H.B. Lau, J.C. Lattanzio, L. Siess, Super and massive AGB stars - II. Nucleosynthesis and yields - Z = 0.02, 0.008 and 0.004. MNRAS **437**(1), 195–214 (2014). https://doi.org/10.1093/mnras/stt1877
166. C.L. Doherty, P. Gil-Pons, H.H.B. Lau, J.C. Lattanzio, L. Siess, S.W. Campbell, Super and massive AGB stars - III. Nucleosynthesis in metal-poor and very metal-poor stars - Z = 0.001 and 0.0001. MNRAS **441**(1), 582–598 (2014). https://doi.org/10.1093/mnras/stu571
167. C.L. Doherty, P. Gil-Pons, L. Siess, J.C. Lattanzio, Super-AGB Stars and their Role as Electron Capture Supernova Progenitors. PASA **34**, e056 (2017). https://doi.org/10.1017/pasa.2017.52
168. M. Limongi, L. Roberti, A. Chieffi, K. Nomoto, Evolution and Final Fate of Solar Metallicity Stars in the Mass Range 7–15 M ⊙. I. The Transition from Asymptotic Giant Branch to Super-AGB Stars, Electron Capture, and Core-collapse Supernova Progenitors. Astrophys. J. Suppl. Ser. **270**(2), 29 (2024). https://doi.org/10.3847/1538-4365/ad12c1. (**ISSN 0067-0049**)
169. E. O'Connor, C.D. Ott, Black Hole Formation in Failing Core-Collapse Supernovae. ApJ **730**(2), 70 (2011). https://doi.org/10.1088/0004-637X/730/2/70
170. M. Limongi, A. Chieffi, Presupernova Evolution and Explosive Nucleosynthesis of Rotating Massive Stars in the Metallicity Range -3 ≤ [Fe/H] ≤ 0. ApJS **237**(1), 13 (2018). https://doi.org/10.3847/1538-4365/aacb24
171. O. Straniero, L. Piersanti, I. Dominguez, A. Tumino, On the Mass of Supernova Progenitors: The Role of the $^{12}C+^{12}C$ Reaction. Nuclei in the Cosmos XV **219**, 7–11 (2019). https://doi.org/10.1007/978-3-030-13876-9_2
172. P. Eggenberger, G. Meynet, A. Maeder, R. Hirschi, C. Charbonnel, S. Talon, S. Ekström, The Geneva stellar evolution code. Ap&SS **316**(1–4), 43–54 (2008). https://doi.org/10.1007/s10509-007-9511-y
173. T. Rauscher, A. Heger, R.D. Hoffman, S.E. Woosley, Nucleosynthesis in Massive Stars with Improved Nuclear and Stellar Physics. ApJ **576**, 323–348 (2002). https://doi.org/10.1086/341728
174. C.A. Meakin, D. Arnett, Active Carbon and Oxygen Shell Burning Hydrodynamics. ApJ **637**(1), L53–L56 (2006). https://doi.org/10.1086/500544
175. C. Ritter, F. Herwig, S. Jones, M. Pignatari, C. Fryer, R. Hirschi, NuGrid stellar data set - II. Stellar yields from H to Bi for stellar models with M_{ZAMS} = 1-25 $M_{\odot}$ and Z = 0.0001-0.02. MNRAS **480**(1), 538–571 (2018). https://doi.org/10.1093/mnras/sty1729
176. R. Andrassy, F. Herwig, P. Woodward, C. Ritter, 3D hydrodynamic simulations of C ingestion into a convective O shell. MNRAS **491**(1), 972–992 (2020). https://doi.org/10.1093/mnras/stz2952
177. F. Rizzuti, R. Hirschi, V. Varma, W.D. Arnett, C. Georgy, C. Meakin, M. Mocák, A. St. John Murphy, T. Rauscher, Shell mergers in the late stages of massive star evolution: new insight from 3D hydrodynamic simulations. arXiv e-prints, art. arXiv:2407.15544, (2024). https://doi.org/10.48550/arXiv.2407.15544
178. L. Roberti, M. Limongi, A. Chieffi, Zero and Extremely Low-metallicity Rotating Massive Stars: Evolution, Explosion, and Nucleosynthesis Up to the Heaviest Nuclei. ApJS **270**(2), 28 (2024). https://doi.org/10.3847/1538-4365/ad1686
179. C. Ritter, R. Andrassy, B. Côté, F. Herwig, P.R. Woodward, M. Pignatari, S. Jones, Convective-reactive nucleosynthesis of K, Sc, Cl and p-process isotopes in O-C shell mergers. MNRAS **474**(1), L1–L6 (2018). https://doi.org/10.1093/mnrasl/slx126
180. L. Roberti, M. Pignatari, A. Psaltis, A. Sieverding, P. Mohr, Z.S. Fülöp, M. Lugaro, The γ-process nucleosynthesis in core-collapse supernovae - i. a novel analysis of γ-process yields in massive stars. A&A **677**, A22 (2023). https://doi.org/10.1051/0004-6361/202346556
181. T. Wang, D. Vartanyan, A. Burrows, M.S.B. Coleman, The essential character of the neutrino mechanism of core-collapse supernova explosions. MNRAS **517**(1), 543–559 (2022). https://doi.org/10.1093/mnras/stac2691
182. L. Boccioli, L. Roberti, M. Limongi, G.J. Mathews, A. Chieffi, Explosion Mechanism of Core-collapse Supernovae: Role of the Si/Si–O Interface. Astrophys. J. **949**(1), 17 (2023). https://doi.org/10.3847/1538-4357/acc06a
183. A.C. Calder, D.M. Townsley, I.R. Seitenzahl, F. Peng, O.E.B. Messer, N. Vladimirova, E.F. Brown, J.W. Truran, D.Q. Lamb, Capturing the fire: flame energetics and neutronization for type iA supernova simulations. Astrophys. J. **656**, 313–322 (2007). https://doi.org/10.1086/510709